Neuropeptide Modulation of Bidirectional Internetwork Synapses

Savanna-Rae H Fahoum

Dawn M Blitz[1]

Running Title: Neuropeptide Modulation of Internetwork Synapses

Department of Biology
Center for Neuroscience and Behavior
Miami University
Oxford OH 45056

[1]Corresponding Author:
Dawn M. Blitz
700 E High St
PSN 212
Oxford OH, 45056
blitzdm@miamoh.edu
513-529-6327

Number of pages: 69
Number of figures: 9 (+ 9 Supplemental Figures)
Number of tables: 6
Number of words
Abstract: 250
New and Noteworthy: 74

Conflict of Interest: The authors declare no competing financial interests.

Acknowledgements: This work supported by the National Science Foundation IOS:1755283 (DMB).

Abstract

Oscillatory networks underlying rhythmic motor behaviors, and sensory and complex neural processing, are flexible, even in their neuronal composition. Neuromodulatory inputs enable neurons to switch participation between networks, or participate in multiple networks simultaneously. Neuromodulation of internetwork synapses can both recruit and coordinate a switching neuron in a second network. We previously identified an example in which a neuron is recruited into dual-network activity via peptidergic modulation of intrinsic properties. We now ask whether the same neuropeptide also modulates internetwork synapses for internetwork coordination. The crab (*Cancer borealis*) stomatogastric nervous system contains two well-defined feeding-related networks (pyloric, food filtering, ~1 Hz; gastric mill, food chewing, ~0.1 Hz). The projection neuron MCN5 uses the neuropeptide Gly^1-SIFamide to recruit the pyloric-only LPG neuron into dual pyloric plus gastric mill-timed bursting via modulation of LPG's intrinsic properties. Descending input is not required for a coordinated rhythm, thus intra-network synapses between LPG and its second network must underlie coordination among these neurons. However, synapses between LPG and gastric mill neurons have not been documented. Using two-electrode voltage clamp recordings, we found that graded synaptic currents between LPG and gastric mill neurons (LG, IC, DG) were primarily negligible in saline, but were enhanced by Gly^1-SIFamide. Further, LPG and gastric mill neurons entrain each other during Gly^1-SIFamide application, indicating bidirectional, functional connectivity. Thus, a neuropeptide mediates neuronal switching through parallel actions, modulating intrinsic properties in a switching neuron to recruit it

into a second network and as shown here, also modulating bidirectional internetwork synapses for coordination.

New and Noteworthy

Neuromodulation can enable neurons to be simultaneously coordinated with separate networks. Both recruitment into, and coordination with, a second network can occur via modulation of internetwork synapses. Alternatively, recruitment can occur via modulation of intrinsic ionic currents. We find that the same neuropeptide previously determined to modulate intrinsic currents also modulates bidirectional internetwork synapses that are typically ineffective. Thus, complementary modulatory peptide actions enable recruitment and coordination of a neuron into a second network.

Keywords: central pattern generator, neuronal switching, graded synaptic transmission, Gly^1-SIFamide

Introduction

Central pattern generators (CPGs) are flexible neuronal networks that each produce different versions of particular rhythmic motor behaviors such as walking, breathing, and chewing (1–5). CPG flexibility includes neuronal switching, in which a neuron changes participation from its “home” network into another, or multiple networks simultaneously, via neuromodulation of synaptic and/or intrinsic properties (6–12). Neuronal switching occurs in invertebrate and vertebrate CPG motor networks, other local oscillatory networks such as in the hippocampus, and is proposed to contribute to larger-scale changes in functional connectivity (10, 13–18). Neuromodulator inputs such as cholinergic basal forebrain and locus coeruleus neurons are implicated in regulating network dynamics on multiple temporal and spatial scales (14, 15, 17, 19). To fully understand how neuromodulatory inputs alter neuronal participation, it is necessary to identify the full complement of modulatory actions enabling a switching neuron to generate activity at the same frequency as a new network and with the correct timing relative to other neurons.

Modulation of internetwork synapses onto a switching neuron recruits a neuron to generate activity at the correct frequency and also enables the correct relative timing (6, 8, 20). In such instances, the switching neuron typically follows the pattern imposed on it, but does not contribute to generating the output pattern in its new network. More recent examples indicate that modulation of intrinsic properties can also regulate neuronal switching (10–12). We found that a neuron recruited to generate activity at a second network frequency via modulation of intrinsic properties can coordinate activity of neurons in the network into which it is recruited (21). For a switching neuron to be

able to coordinate activity in the new network, one possibility is that there are functional synapses already present, and bursting of the switching neuron at the second frequency simply has effects via those existing synapses. An alternative possibility is that there are not functional synapses to mediate coordination under unmodulated conditions, and modulation of synapses is required to enable coordination between a switching neuron and other neurons in its new network. This suggests that in contrast to modulation of internetwork synapses enabling a neuron to generate activity at the correct frequency and with the correct relative timing, modulation of intrinsic properties may require complementary modulatory actions. Here, we tested the hypothesis that modulation of synapses occurs between a switching neuron and its new network neurons, as a complement to the modulation of intrinsic properties that enable a switching neuron to exhibit dual frequency bursting.

In the STNS of the crab, *Cancer borealis*, activation of the modulatory commissural neuron 5 (MCN5) causes the pyloric-only LPG neuron to switch into dual pyloric- and gastric mill-timed bursting (12, 21). The LPG switch into gastric mill bursting occurs due to the MCN5 neuropeptide Gly^1-SIFamide modulating a hyperpolarization-activated current, a persistent sodium current, and calcium, or calcium-related current(s) (12, 22). As part of our investigation into how the MCN5-elicited rhythm is generated, we found that LPG gastric mill-timed (slow) bursting is regulated by gastric mill network neurons, and that LPG can contribute to coordination among gastric mill network neurons (21), suggesting bidirectional communication between the LPG switching neuron and at least some of the gastric mill network neurons. However, in unmodulated saline conditions synapses between LPG and LG, IC, and DG gastric mill neurons have

119 not been described. Therefore, we used two-electrode voltage clamp recordings to
120 investigate whether there are functional synapses in the control saline condition, and
121 whether the neuropeptide Gly^1-SIFamide modulates synaptic transmission between
122 LPG and LG, IC, and DG neurons, in addition to its established modulation of LPG's
123 intrinsic properties. We further tested for connectivity among the neurons by assessing
124 the ability of LPG, LG, IC, and DG to entrain each other during Gly^1-SIFamide
125 application.
126

127 **Materials and methods**

128 Animals

129 Male *Cancer borealis* crabs were obtained from The Fresh Lobster company
130 (Gloucester, MA) and maintained in tanks containing artificial seawater at 10-12 °C. For
131 experiments, crabs were anesthetized on ice for 30-50 min, then during gross
132 dissection, the foregut was removed from the animal, bisected, and pinned flat in a
133 Slygard-170-lined dish (Thermo Fisher Scientific). During fine dissection, the
134 stomatogastric nervous system (STNS) was dissected from the foregut and pinned in a
135 Sylgard 184-lined petri dish (Thermo Fisher Scientific) (23). During the dissection, the
136 preparation was kept chilled in *C. borealis* physiological saline at 4 °C.
137

138 Solutions

139 *C. borealis* physiological saline was composed of the following (in mM): 440
140 NaCl, 26 $MgCl_2$,13 $CaCl_2$,11 KCl,10 Trizma base, 5 Maleic acid, pH 7.4-7.6. Squid
141 internal electrode solution contained the following (in mM): 10 $MgCl_2$, 400 Potassium D-

142 gluconic acid, 10 HEPES, 15 Na_2SO_4, 20 NaCl, pH 7.45 (24). Gly^1-SIFamide
143 (GYRKPPFNG-SIFamide, custom peptide synthesis: Genscript) (12, 25–28) was
144 dissolved in optima water (Thermo Fisher Scientific) at 10^{-2} M and stored at -20 °C.
145 Tetrodotoxin (TTX) powder was dissolved in optima water at a final concentration of 10^{-4}
146 M and stored at -20 °C. Stock solution of picrotoxin (PTX) was made by adding PTX
147 powder (Sigma Aldrich) to 95% ethanol at 10^{-2} M and storing at -20 °C. For experiments,
148 each substance was thawed and diluted in physiological saline at a final concentration
149 of: Gly^1-SIFamide, 5 μM; TTX, 1 μM and 0.1 μM; PTX, 10 μM.
150

151 Electrophysiology

152 All preparations were continuously superfused with chilled *C. borealis* saline (8-
153 10 °C), or chilled saline containing Gly^1-SIFamide, PTX, and/or TTX, as indicated. For
154 uninterrupted superfusion of the preparation, all solution changes were performed using
155 a switching manifold. Extracellular nerve activity was recorded using a model 1700 A-M
156 Systems Amplifier and custom-made stainless-steel pin electrodes. Vaseline wells were
157 built around nerves to isolate neuron signals, with one stainless-steel electrode wire
158 placed inside the well, and the other outside the well as reference. Stomatogastric
159 ganglion (STG) somata were exposed by removing the thin layer of tissue across the
160 ganglion and observed with light transmitted through a dark-field condenser (MBL-
161 12010 Nikon Instruments). Intracellular recordings were collected using sharp-tip glass
162 microelectrodes (18 – 40 MΩ) filled with squid internal electrode solution for entrainment
163 experiments or filled with 0.6 M K_2SO_4 plus 20 mM KCl electrode solution for voltage
164 clamp experiments. STG neurons and their locations were identified based on their

165 intracellular activity, nerve projection patterns, and their interactions with other STG
166 neurons. All intracellular recordings were collected using AxoClamp 900A amplifiers in
167 current-clamp mode for entrainment experiments or two-electrode voltage clamp
168 (TEVC)-mode for synapse experiments (Molecular Devices). All experiments were
169 conducted in the isolated STNS following transection of the inferior and superior
170 oesophageal nerves (*ion* and *son*, respectively). Electrophysiology recordings were
171 collected using data acquisition hardware (Entrainment experiments: Micro1401,
172 Cambridge Electronic Design; Synapse experiments: DigiData 1440A, Molecular
173 Devices), software (Entrainment experiments: Spike2, ~5 kHz sampling rate, Cambridge
174 Electronic Design; Synapse experiments: Clampex 10.7, Molecular Devices, ~5 kHz
175 sampling rate) and laboratory computer (Dell).
176 Prior to all conducted experiments, unless otherwise indicated, the LP neuron
177 was photoinactivated for the established bath-application model of MCN5 actions (12).
178 Briefly, the LP neuron was impaled with a sharp microelectrode (30-40 MΩ) that was
179 tip-filled with AlexaFluor-568 hydrazide (10 mM in 200 mM KCl, Thermo Fisher
180 Scientific) and back-filled with squid internal solution (see *Solutions*). The LP soma was
181 filled using constant hyperpolarizing current injection (-5 nA) for 5-10 min, and the
182 current injection removed to allow the dye to diffuse to the neurites and axon in the *dvn*
183 for 20 – 40 min. The STG was then illuminated for 5 – 7 min using a Texas red filter set
184 (560 ± 40 nm wavelength; Leica Microsystems). Complete photoinactivation was
185 confirmed when the LP membrane potential reached 0 mV.
186

187 Graded synapses via two-electrode voltage clamp

188 To determine whether graded synapses between LPG and gastric mill neurons
189 were present and/or modulated by Gly^1-SIFamide, we used two-electrode voltage clamp
190 (TEVC) recordings. Based on previous studies, we only proceeded with experiments
191 and analyzed data when pre- and post-synaptic cells had an input resistance of at least
192 10 MΩ (24, 29). Action potentials were blocked with TTX (initial concentration: 1 μM,
193 ~5-10 min; final maintained concentration: 0.1 μM). When IC, LG, or DG was the
194 presynaptic neuron, they were voltage clamped at -60 mV. The presynaptic neuron was
195 stepped from its holding potential to -55 to -20 mV in 5 mV increments (5 s duration, 11
196 s inter-step interval). The postsynaptic cell was voltage clamped at -40 mV. For IC, LG,
197 and DG to LPG synapses, the voltage step protocol was repeated in Gly^1-SIFamide
198 (SIF, 5 μM) plus TTX (0.1 μM) (TTX:SIF), following ~10 min wash-in of TTX:SIF. To
199 measure potential LPG to IC, LG, or DG synapses, the same voltage step protocol was
200 used, however, PTX (10 μM) was used to block glutamatergic inhibitory synapses. LPG
201 uses acetylcholine as its transmitter, and thus its actions are not blocked by PTX (30–
202 32), enabling us to examine synapses from LPG onto LG, IC, and DG more directly.
203 When LPG was the presynaptic neuron, it was held at -80 mV to turn off spontaneous
204 activity of the other non-clamped LPG neuron. In TTX:PTX:Saline LPG was stepped
205 from its holding potential to -55 mV to -20 mV in 5 mV increments, and the postsynaptic
206 neuron current recorded with cells at a holding potential of -40 mV. This protocol was
207 repeated in Gly^1-SIFamide in TTX plus PTX (TTX:PTX:SIF), following ~10 min wash-in
208 of TTX:PTX:SIF. In a small subset of experiments as indicated, each presynaptic
209 neuron (LG, IC, DG, or LPG), was clamped at a holding potential of -80 mV and

210 stepped from -70 mV to -20 mV in 5 mV increments. Between each experimental
211 condition, all neurons were held at -60 mV, near resting potential for STG neurons (33).
212 Due to a factor of 10 error in a gain setting in TEVC in one amplifier, current amplitudes
213 were multiplied post-hoc by a factor of 10. Before any adjustments were made, input
214 resistance measurements in current clamp mode, unaffected by the gain error, from
215 pre- and post-TEVC mode were compared to input resistance measurements in TEVC
216 mode to verify the gain factor error. Additionally, the same neuron (e.g., LG) was not
217 always recorded using the channel with the gain error in different preparations. Adjusted
218 data matched the data recorded with the correct conversion factor in other experiments.
219 Voltage step protocols were repeated five times in each direction during each
220 pair of synapses tested. Recordings were averaged and filtered using Clampfit 10.7
221 (pClamp, Molecular Devices, San Jose, CA) prior to analysis. Synaptic currents were
222 measured by subtracting the mean holding current during the 2 s preceding each
223 voltage step (Baseline) from the peak current within the first 2 s of the voltage step
224 (Early) and the last 2 s of the voltage step (Late). For LPG to IC and to LG, we observed
225 an inward current within the first 2 s of each voltage step. Thus, we also measured the
226 peak amplitude of this inward current and subtracted it from the mean holding current.
227
228 Gastric mill network entrainment
229 To examine whether each gastric mill-timed network neuron entrained each
230 other, entrainment neurons (LPG [two copies], LG, IC, and DG [one copy each]) were
231 stimulated with rhythmic depolarizing current injections (5 s pulse duration, 0.5 to 6 nA)
232 at different entrainment frequencies (0.03 – 0.12 Hz; 5 s pulse, 6 to 28 s inter-pulse

233 interval). Entrainment frequency started at 0.3 Hz or the first frequency (in 0.1 Hz
234 increments) at which a neuron was able to be entrained. The amount of current injected
235 into the entrainment neuron was chosen to match the firing frequency (± 5 Hz) of that
236 neuron at steady state Gly^1-SIFamide application prior to initiating entraining
237 depolarizations. In some preparations, the entraining neuron was not active in Gly^1-
238 SIFamide, and we matched its firing frequency to the entraining neuron mean firing
239 frequency from a previous data set (21). All entrainment manipulations were conducted
240 during the last 20 min of a 30 min Gly^1-SIFamide (5 μM) application. To examine LPG
241 entrainment of gastric mill neurons LG, IC, and DG more directly, we performed an
242 additional set of experiments in which picrotoxin (PTX, 10 μM), which blocks LG, IC,
243 and DG glutamatergic inhibitory synapses, but not cholinergic LPG synapses (30–32),
244 was added to the saline and Gly^1-SIFamide (SIF:PTX) solutions. This condition isolates
245 LPG from gastric mill input and blocks chemical synapses among the LG, IC, DG,
246 neurons (30–32).
247 For each entrainment frequency, either the single LG, IC, or DG neuron, or both
248 LPG neurons were rhythmically depolarized for ten cycles (11 bursts), and the
249 instantaneous gastric mill burst frequency (1/cycle period [time between the first action
250 potentials of two consecutive bursts]) for each test neuron (LG, IC, DG, and LPG) was
251 measured. For LPG and IC, which can participate in both the pyloric and gastric mill
252 rhythms, only gastric mill-timed bursts (defined below in Gastric mill burst identification)
253 were used in analyses.
254

255 Integer coupling analysis

256 To quantify the extent of entrainment between LG and IC, DG, and LPG, we
257 used integer coupling as a measure of whether there was a fixed relationship between
258 the instantaneous burst frequencies of each pair of neurons (34, 35). Integer coupling
259 was measured by dividing the entraining neuron stimulation frequency by the
260 instantaneous test neuron burst frequency and extracting the significand (the value to
261 the right of the decimal point) from each ratio at each entrainment frequency, across
262 preparations. The significand indicates a measure of how close a ratio is to an integer.
263 For instance, if the ratio between the entrainment and instantaneous burst frequencies
264 is 1.01, then significand is 0.01 and close to zero. If the ratio is 1.99, then the significand
265 is 0.99 and close to 1. The cumulative probability distribution frequency (c.d.f.) of all
266 significands for each entrainment frequency was calculated to determine how close
267 each set of ratios was to an integer and plotted on a histogram. The shaded regions
268 indicate the c.d.f. curves between entraining and test neurons at 0.06 Hz entrainment
269 frequency (Figs. 6D, 7-8Ai, Bi). The blue dotted line indicates one extreme of perfect
270 integer coupling, where all significands from all ratios are near 0 or 1, and the c.d.f.
271 accumulates primarily at 0 or 1 (Figs. 6D, 7-8Ai, Bi) (35). On the other hand, if all
272 significands across a group of data points are randomly and uniformly distributed
273 between 0 and 1, then the c.d.f. of these values would be close to a diagonal line, and
274 thus indicate zero integer coupling between neurons (solid red y = x line, Figs. 6D, 7-
275 8Ai, Bi) (35).

276 To quantify the extent of integer coupling at each entrainment frequency, that is,
277 the distance between the cumulative distribution and a random distribution (i.e., a

diagonal line), we calculated the area between each c.d.f. curve and the diagonal line using a custom-written MATLAB script (MathWorks). For instance, if there was perfect integer coupling at a particular entrainment frequency, then the area between a c.d.f. falling along the blue dotted line and the diagonal would be 0.25, while an area close to zero would suggest there is no integer coupling between the entrainment and test neurons. To determine whether significands from a group of entrainment frequencies were significantly different from the diagonal line, we formulated a uniform distribution that would equal the y = x diagonal line, and thus have an area equal to zero to indicate no integer coupling. Then, for each entrainment frequency, we compared the experimental data to the uniform distribution using a two-sample Kolmogorov-Smirnov test (35). We used a two-sample test instead of a one-sample test because the calculated significands for the experimental data cannot be expected to be normally distributed (35). We divided the significance level by the number of entrainment frequencies (7) to correct for multiple comparisons. Thus, our significance threshold was 0.05/7 = 0.007. Entrainment frequencies with data from only one preparation were excluded from the integer coupling analysis.

The integer coupling analysis assumes test neuron integer-multiple relationships to the entrainment neuron (e.g., 1:1, 2:1, 3:1) using test neuron/entrainment neuron ratios. However, we did observe some fractional relationships in which there are fewer test neuron cycles relative to entrainment neuron (e.g., 1:2, 1:3; Fig. 6Biii). These entrainment relationships would result in significands between 0 and 1, for example a 1:2 entrainment would result in a significand of 0.5. The example “perfect” entrainment area of 0.25 (area between blue and red lines in figure 6D), represents equal

301 proportions of significands occurring close to 0 or 1. Although the area calculation for
302 “perfect” entrainment at intermediate significand values would differ from 0.25, it should
303 still be greater than 0 and thus our area measurement enables us to quantify whether
304 entrainment occurred, regardless of the type of entrainment.
305

306 Gastric mill neuron burst identification

307 Only neurons that were bursting in gastric mill time during entrainment
308 stimulations were included in the entrainment plots and integer coupling analysis.
309 Criteria to determine gastric mill-timed bursting included: IC bursts had a duration of at
310 least 0.45 s, with consecutive pyloric-timed IC bursts with burst durations of at least
311 0.45 s grouped together into a gastric mill burst, including up to one IC burst < 0.45 s in
312 duration if it occurred between other IC bursts that were at least 0.45 s (21, 28); LG and
313 DG bursts had at least 3 spikes per burst with a maximum 2 s interspike interval; and
314 LPG gastric mill-timed bursts were identified as described (12). Briefly, a histogram
315 containing LPG interspike intervals (ISIs) across an entire Gly^1-SIFamide application
316 was generated using a custom-written MATLAB script and the two largest peaks
317 identified. The mean ISI between the first peak (~0 – 0.5 s, intraburst intervals) and
318 second peak (~0.5 – 2 s, interburst intervals) was calculated and used as a cutoff value
319 to identify LPG bursts, such that an ISI above the cutoff indicated the end of one burst
320 and the beginning of another. A custom written Spike2 script that identifies LPG bursts
321 with a duration greater than one pyloric cycle period (from PD burst onset to the next
322 PD burst onset, ~1 s) was then used to select only LPG gastric mill bursts from all LPG
323 bursts identified with the ISI cutoff (12).

324

325 Software and Statistics

326 Raw electrophysiology data were analyzed using Clampfit 10.7, as well as
327 functions and scripts that were written in Spike2 and MATLAB. Graphs were plotted in
328 SigmaPlot (Systat) or MATLAB and imported into CorelDraw (Corel). All final figures
329 were created using CorelDraw. Statistical analyses were performed using SigmaPlot or
330 MATLAB. Data were analyzed for normality using Shapiro-Wilk test before determining
331 whether to use a parametric or nonparametric test on each dataset. A two-sample
332 Kolmogorov-Smirnov test was used for integer coupling analysis. Two-way repeated
333 measures (RM) analysis of variance (ANOVA) and Holm-Sidak post hoc tests for
334 multiple comparisons were used for synaptic current analyses. Threshold for
335 significance was $p < 0.05$, except for integer coupling analysis which had a threshold of
336 $p < 0.007$. All data are presented as mean ± SEM.

337

338 Code Accessibility

339 Scripts and functions used for analysis were written in Spike2 and/or MATLAB
340 and are available at https://github.com/blitzdm/Fahoum_Blitz_2023_Synapses or upon
341 request from D.M.B.

342

343 **Results**

344 The crustacean stomatogastric nervous system (STNS) is a region of the central
345 nervous system that controls feeding-related movements of the foregut, including the
346 pyloric (food filtering, ~1 Hz) and gastric mill (food chewing, ~0.1 Hz) rhythms (36, 37)

347 (Fig. 1A). The STNS is comprised of the paired commissural ganglia (CoG), single
348 oesophageal ganglion (OG), the single stomatogastric ganglion (STG), and their
349 connecting and peripheral nerves (Fig. 1A). The STG contains ~30 neurons contributing
350 to well-characterized CPG networks which drive the pyloric and gastric mill rhythms
351 (Fig. 1B). Modulatory projection neurons originating in the CoGs and OG project to the
352 STG where they alter intrinsic properties of individual neurons and/or the synapses
353 between them to elicit multiple different versions of each rhythm (38–40).
354 The projection neuron modulatory commissural neuron 5 (MCN5) is located in the
355 CoG and projects its axons to the STG via the inferior oesophageal and stomatogastric
356 nerves (*ion* and *stn*, respectively; Fig. 1A). Bath application or neuronal release of the
357 MCN5 neuropeptide Gly^1-SIFamide increases pyloric frequency (41) and activates the
358 gastric mill rhythm (12, 28). Furthermore, MCN5 activation or bath application of its
359 neuropeptide Gly^1-SIFamide (5 μM) switches the LPG neuron from pyloric-only activity
360 to dual pyloric/gastric mill-timed bursting (fast/slow, respectively) (12, 21, 28). LPG is
361 active in pyloric time due to electrical coupling to the other pyloric pacemaker neurons
362 (AB, PD; Fig. 1B) and generates slower, gastric mill-timed bursts due to Gly^1-SIFamide
363 modulation of LPG intrinsic properties (12, 22). Although the LPG gastric mill-timed
364 bursting does not require synaptic input from the gastric mill network, these oscillations
365 are regulated by gastric mill network neurons including being coordinated with the rest
366 of the gastric mill network. Further, LPG slow bursting regulates LG and dorsal gastric
367 (DG) neuron activity, and LPG can coordinate gastric mill network neurons (21),
368 suggesting the presence of synapses between LPG and the gastric mill neurons.
369 Synapses between LPG and gastric mill network neurons have not been described (Fig.

370 1B) (42). We hypothesized that Gly^1-SIFamide modulates synapses between LPG and
371 LG, IC, and DG to become functional in this particular modulatory state.
372
373 Gly^1-SIFamide modulates synapses between LG and LPG
374 Among STG neurons, neurotransmitter release is primarily controlled in a graded,
375 voltage-dependent manner by subthreshold membrane potential oscillations (43–46).
376 Therefore, we used two-electrode voltage clamp (TEVC) recordings in pairs of neurons
377 (LPG:LG, LPG:IC, and LPG:DG), in TTX (0.1 μM) to block action potentials, and
378 examined whether a synaptic current was elicited in response to presynaptic voltage
379 steps.
380 We first examined whether there was a graded synapse from LG to LPG. LG was
381 voltage clamped at -60 mV and stepped from -55 mV to -20 mV in 5 mV increments (5 s
382 duration, 11 s inter-step interval) and LPG was voltage clamped at -40 mV (Fig. 2A). In
383 TTX:Saline, there was no apparent synaptic current elicited in LPG, suggesting that
384 there was no functional synapse from LG to LPG in saline conditions (Fig. 2A, black
385 traces). When TTX plus Gly^1-SIFamide (TTX:SIF) was applied to the preparation, an
386 outward current was evoked during LG voltage steps, with increased amplitude at more
387 depolarized voltage steps (Fig. 2A, red traces). Additionally, we observed “bumps” in
388 the LPG synaptic currents, such as in the grey trace, that were similar to transient
389 currents that we observed between LG voltage steps (Fig. 2A, grey arrows, n = 4/4
390 preparations). We hypothesized that these “bumps” reflect synaptic input due to Gly^1-
391 SIFamide-elicited activity in the DG and/or IC neuron. However, the early outward
392 current (during the “Early” bracket), which increased in amplitude with greater

393 depolarization of the LG neuron, was consistently time-locked to the LG voltage steps,
394 and is thus a synaptic current elicited by depolarization of the LG neuron (Fig. 2A, red
395 traces). To quantify the LPG response to LG voltage steps, we subtracted the mean
396 holding current (Baseline) across two seconds immediately prior to the voltage step
397 from the peak amplitude of LPG current within the first two seconds of the voltage step
398 (Early) and the last two seconds of the voltage step (Late) (Fig. 2A, blue brackets). LPG
399 synaptic current was plotted as a function of LG voltage steps for each of the two
400 measurement time points (Fig. 2Bi-Bii; TTX:Saline black symbols, TTX:SIF red symbols;
401 each symbol represents one experiment). We used a two-way repeated measures (RM)
402 ANOVA for statistical analysis with condition (TTX:Saline vs. TTX:SIF), and voltage as
403 the two main effects. For the LPG synaptic current during the first 2 s, there was a
404 significant interaction of condition and voltage (Fig. 2Bi) ($F[3,7] = 2.92$, $p = 0.027$, Two
405 Way RM ANOVA; $n = 4$). Specifically, the peak current amplitude was different between
406 TTX:Saline and TTX:SIF between -35 and -20 mV, except for -30 mV (Table 1; $n = 4$).
407 As a graded synaptic current should express voltage-dependence, we used a
408 comparison of the measured current between -55 and -20 mV for an indicator of
409 voltage-dependence. There was no difference in current between these two voltages in
410 the TTX:Saline condition, but there was a larger current at -20 mV compared to -55 mV
411 in the TTX:SIF condition (Table 1; $n = 4$). During the last 2 s of each LG voltage step,
412 there was also a significant interaction between condition and voltage on the LPG
413 synaptic current (Fig. 2Bii) ($F[3,7] = 5.01$, $p = 0.002$, Two Way RM ANOVA, $n = 4$).
414 There was a larger LPG synaptic current during Gly^1-SIFamide compared to TTX:Saline
415 during LG depolarizing steps from -35 to -20 mV (Table 1; $n = 4$). Similar to the first 2 s,

416 there was no voltage-dependence in TTX:Saline during the last 2 s of the voltage steps,
417 but there were differences in the synaptic current amplitudes between -55 and -20 mV
418 during TTX:SIF (Table 1; n = 4). Thus, Gly^1-SIFamide enhanced a synapse from LG to
419 LPG, which was dependent upon presynaptic voltage, that was not evident in the
420 TTX:Saline condition.

421 We next tested for a synaptic connection from LPG to LG. TTX was applied with
422 picrotoxin (PTX, 1 μM) to block LG, IC, and DG inhibitory glutamatergic synapses to
423 examine LPG cholinergic synapses onto LG without complications of chemical
424 transmission from the other gastric mill neurons that were not voltage clamped. Since
425 we performed TEVC with only one of the two LPG neurons, LPG was voltage clamped
426 at -80 mV to eliminate spontaneous bursting activity of the other non-clamped LPG
427 neuron between voltage steps. The voltage-clamped LPG neuron was stepped from its
428 holding voltage to -55 to -20 mV in 5 mV increments, or in a subset of experiments to
429 additional voltage steps ranging from -70 mV to -20 mV (5 s duration, 11 s inter-step
430 interval) (Fig. 2C). LG was voltage clamped at -40 mV. In saline conditions, during LPG
431 voltage steps, a series of small amplitude, inward currents were evoked in LG (Fig. 2C,
432 black traces, black arrows). During application of Gly^1-SIFamide, there was still an initial
433 inward current in LG within the first two seconds of each LPG voltage step, but the small
434 repetitive currents were then summed with a larger amplitude outward current (Fig. 2C,
435 red traces). The outward current in LG increased with increasing LPG voltage steps,
436 indicating graded transmitter release (Fig. 2C, red traces).

437 We quantified LG synaptic current from LPG in the same way as described above at
438 the Early and Late time points, with LG synaptic current plotted as a function of LPG

439 voltage steps (Fig. 2Di-Dii). For the peak LG synaptic current during the Early part of the
440 voltage step, there was no significant interaction of condition and voltage (Fig. 2Di)
441 ($F[3,7] = 2.267$, $p = 0.069$), nor a main effect of voltage ($F[3,7] = 1.61$, $p = 0.187$) or
442 condition ($F[3,1] = 3.95$, $p = 0.141$; Two-way RM ANOVA; $n = 4$). However, during the
443 Late part of each LPG voltage step, there was a significant interaction between
444 condition and voltage (Fig. 2Dii) ($F[3,7] = 5.11$, $p = 0.002$, Two-way RM ANOVA; $n = 4$).
445 Specifically, the peak LG synaptic current amplitude was different between TTX:Saline
446 and TTX:SIF between -35 and -20 mV (Fig. 2Dii; Table 1; $n = 4$). Further, the synaptic
447 current amplitudes were different between -55 and -20 mV in TTX:SIF (Table 1; $n = 4$)
448 indicating voltage-dependence, but not during TTX:Saline (Table 1; $n = 4$). Thus, the
449 LPG to LG current appeared to have a slower onset than the LG to LPG synaptic
450 current as there was only a significant increase in current in the Late component of the
451 LPG voltage step (Fig. 2Dii). In the STNS, cholinergic inhibition has a slower time
452 course than glutamatergic inhibition (32, 47, 48), aligning with the apparent differences
453 in timing between the LG- (glutamatergic) and LPG- (cholinergic) elicited synaptic
454 currents.
455 Unlike the outward current elicited in LG, the inward current was not voltage
456 dependent or modulated by Gly^1-SIFamide. As the inward current summed with the
457 outward current beyond the beginning of the voltage step, we only quantified its
458 amplitude during the initial 2 s period. We found no interaction between condition and
459 voltage ($F[1,7] = 0.34$, $p = 0.911$), and no effect of condition ($F[1,1] = 3.25$, $p = 0.071$) or
460 voltage ($F[1,7] = 0.71$, $p = 0.554$; Two-way RM ANOVA, $n = 4$).
461

462 Gly[1]-SIFamide modulates synapses between IC and LPG

463 We next examined whether a graded synapse was present from IC to LPG. Using
464 the same protocol as above, in TTX:Saline, IC voltage steps elicited a small outward
465 current during steps from -35 to -20 mV indicating a functional synapse between IC and
466 LPG in Saline (Fig. 3A, black traces, n = 5/5). When TTX:SIF was applied to the
467 preparation, a larger outward current was evoked during IC voltage steps, with
468 increased amplitude at more depolarized voltage steps (Fig. 3A, red traces). Similar to
469 the LPG synaptic current from LG voltage steps, we observed that the LPG outward
470 synaptic current had a steep slope as it reached its peak in the first two seconds of IC
471 voltage steps at the more depolarized voltages (Fig. 3A, red traces). In 5/5 preparations,
472 we observed “bumps” in LPG synaptic current during IC voltage steps that appeared
473 similar to those observed during LG voltage steps (Fig. 3A, red trace, grey arrows).
474 However, these currents occurred only during IC voltage steps, not when IC was held at
475 -60 mV.

476 Across preparations, during the Early time point of the LPG synaptic current,
477 there was a significant interaction of condition and voltage (Fig. 3Bi) ($F[4,7] = 3.81$, $p =$
478 0.005; Two-way RM ANOVA; n = 5). Specifically, the peak LPG current amplitude was
479 different between TTX:Saline and TTX:SIF between -35 and -20 mV (Table 2; n = 5). In
480 addition, there was a difference in the LPG synaptic current amplitude between -55 mV
481 and -20 mV in TTX:SIF, but not during TTX:Saline (Table 2; n = 5). During the Late time
482 window of each IC voltage step, there was also a significant interaction between
483 condition and voltage on the LPG synaptic current (Fig. 3Bii) ($F(4, 7) = 5.07$, $p < 0.001$;
484 Two-way RM ANOVA; n = 5). LPG synaptic current was larger during TTX:SIF

485 compared to TTX:Saline during IC depolarizing voltage steps between -35 and -20 mV
486 (Table 2; n = 5). Similar to the Early component, there was no voltage dependence in
487 TTX:Saline during the Late component of the IC voltage steps, but the LPG synaptic
488 current amplitude was different between -55 mV and -20 mV during TTX:SIF (Table 2; n
489 = 5). Thus, there were synaptic currents present in the Saline condition, and Gly^1-
490 SIFamide enhanced this synapse from IC to LPG.

491 We also found a modulated synapse in the opposite direction, from LPG to IC. As
492 explained above, LPG was voltage clamped at -80 mV and stepped from -70 to -20 mV
493 or from -55 to -20 mV in 5 mV increments (Fig. 3C-D), with PTX included to block
494 glutamatergic transmission. IC was voltage clamped at -40 mV. In saline conditions, IC
495 responded to LPG voltage steps by generating a small amplitude, downward peak (Fig.
496 3C, black traces, black arrows, n = 4/5). During Gly^1-SIFamide plus TTX:PTX
497 application, there was still an initial downward response (inward, excitatory current, n =
498 5/5) in the first two seconds of each LPG voltage step with a subsequent outward
499 inhibitory current in IC that increased with more depolarized LPG voltage steps,
500 suggesting that LPG inhibited IC in a graded manner (Fig. 3C, red traces).

501 Across experiments, there was an increased amplitude of LPG-elicited synaptic
502 current in IC, with a presynaptic voltage-dependence, in Gly^1-SIFamide. For the IC
503 synaptic current in the Early component of each LPG voltage step, there was a
504 significant interaction of condition and voltage (Fig. 3Di) ($F[4,7] = 6.57$, $p < 0.001$; Two-
505 way RM ANOVA; n = 5). The Early IC synaptic current amplitude was different between
506 TTX:PTX:Saline and TTX:PTX:SIF from -50 to -20 mV (Table 2; n = 5). Furthermore,
507 there was a difference in the IC current amplitude at -55 vs. -20 mV in TTX:PTX:SIF, but

508 not during TTX:PTX:Saline (Table 2; n = 5). During the Late component of LPG voltage
509 steps, there was also a significant interaction between condition and voltage (Fig. 3Dii)
510 ($F[4,7] = 10.75$, $p < 0.001$; Two-way RM ANOVA; n = 5). There was a larger IC synaptic
511 current during TTX:PTX:SIF compared to TTX:PTX:Saline during LPG depolarizing
512 voltage steps from -55 to -20 mV (Table 2; n = 5). Furthermore, IC synaptic current
513 amplitude during the Late component displayed voltage dependence during
514 TTX:PTX:SIF application, but not during TTX:PTX:Saline (-55 vs -20 mV; Table 2; n =
515 5).
516 We also measured the peak inward current in IC in saline and Gly^1-SIFamide
517 conditions. We found an effect of condition ($F[4,1] = 11.85$, $p = 0.026$) and LPG voltage
518 ($F[4,7] = 7.13$, $p < 0.001$), but no interaction between condition and voltage ($F[4,7] =$
519 1.28, $p = 0.299$; Two-way RM ANOVA; n = 5). In conclusion, these results suggest that
520 a voltage dependent inhibitory graded synapse from LPG onto IC was not functional in
521 baseline condition but was enhanced by Gly^1-SIFamide. For this pair, there was little
522 difference in the Early vs. Late components, however in the example traces (Fig. 3C),
523 the rise time of the IC synaptic current does appear slower than the rise time of the IC to
524 LPG synapse (Fig. 3A).
525
526 <u>Gly^1-SIFamide modulates synapses between DG and LPG</u>
527 For the last pair of neurons, DG and LPG, there was no apparent synaptic current
528 elicited in LPG in an example experiment in TTX:Saline (Fig. 4A, black traces). When
529 TTX:SIF was applied to the preparation, a small outward current was evoked during DG
530 voltage steps, but the amplitude did not appear to change with more depolarized

531 voltage steps (Fig. 4A, red traces). Although small, at more depolarized DG voltages (-
532 25 to -20 mV), the LPG outward synaptic current reached its peak rapidly (Fig. 4A, red
533 traces), compared to the example LPG to DG synaptic currents (Fig. 4C).

534 With one exception, DG to LPG synaptic currents were small relative to those
535 elicited by IC and LG voltages (Figs. 2-4). Using the same quantification of synaptic
536 currents as above, we found for the Early LPG synaptic current, there was only an effect
537 of voltage (Fig. 4Bi) ($F[3, 7] = 4.86$, $p = 0.002$, Two-way RM ANOVA; n = 4), such that
538 the LPG synaptic current amplitude was different between -55 vs. -20 mV during
539 TTX:SIF, but not during TTX:Saline (Table 3; n = 4). There was no effect of condition
540 ($F[3, 1] = 4.58$, $p = 0.122$), nor interaction between condition and voltage on LPG
541 current during the Early component ($F[3, 7] = 0.98$, $p = 0.475$; Two-way RM ANOVA; n
542 = 4). Similarly, during the Late component of each DG voltage step, there was an effect
543 of voltage (Fig. 4Bii) ($F[3,7] = 6.79$, $p < 0.001$; Two-way RM ANOVA; n = 4), such that
544 there were differences in LPG synaptic current amplitudes between DG voltage steps to
545 -55 vs. -20 mV in TTX:SIF, but not during TTX:Saline (Table 3; n = 4). However, there
546 was no effect of condition ($F[3, 1] = 5.34$, $p = 0.104$), nor an interaction between
547 condition and voltage ($F[3, 7] = 1.88$, $p = 0.132$; Two-way RM ANOVA; n = 4). Overall,
548 although there was no statistical difference between saline and Gly^1-SIFamide
549 conditions, there was a voltage-dependent effect on LPG current only during Gly^1-
550 SIFamide. This suggests that the Gly^1-SIFamide peptide did modulate a DG-to-LPG
551 synapse that was not effective at baseline, however the peptide effects were quite
552 variable. The effects on the DG to LPG synaptic currents included a quadrupling of

553 current amplitude (n=1/4), no change in amplitude (n = 1/4) and a small but evident
554 increase in strength (n = 2/4; Fig. 4A, Bi). We did not explore this variability further.
555 Lastly, we tested whether a graded synapse from LPG to DG was present. In
556 TTX:PTX:Saline, DG current did not appear to change relative to baseline current,
557 suggesting that there was no functional synapse between LPG and DG in saline
558 conditions (Fig. 4C, black traces). During Gly^1-SIFamide application, DG generated an
559 outward inhibitory current that increased with increasing LPG voltage steps, suggesting
560 that LPG inhibited DG in a graded manner (Fig. 4C, red traces). As in LG and IC, the
561 LPG-elicited synaptic current in DG had a slower time-course than the DG to LPG
562 synaptic current.
563 Quantification and statistical analysis across experiments supported modulation
564 of an LPG to DG synapses as in the example experiment. For the Early component of
565 the DG synaptic current, there was a significant interaction of condition and voltage (Fig.
566 4Di) ($F[4, 7] = 4.45$, $p = 0.002$; Two-way RM ANOVA; n = 5). Specifically, the Early DG
567 synaptic current amplitude was different between TTX:PTX:Saline and TTX:PTX:SIF
568 between -35 and -20 mV, except for -30 mV (Table 3; n = 5). Furthermore, there was a
569 difference in the DG synaptic current amplitude at -55 vs. -20 mV in TTX:PTX:SIF, but
570 not during TTX:PTX:Saline (Table 3; n = 5). During the Late component of each LPG
571 voltage step, there was also a significant interaction of condition and voltage (Fig. 4Dii)
572 ($F[4, 7] = 6.49$, $p < 0.001$; Two-way RM ANOVA; n = 5). There was a larger DG synaptic
573 current during TTX:PTX:SIF compared to TTX:PTX:Saline during LPG depolarizing
574 steps from -40 to -20 mV (Table 3; n = 5). Additionally, voltage dependence of the DG
575 synaptic current amplitudes was evident during TTX:PTX:SIF, but not during

576 TTX:PTX:Saline (-55 vs. -20 mV; Table 3; n = 5). Thus, Gly^1-SIFamide enhanced a
577 synapse from LPG to DG, which was dependent upon presynaptic voltage, that was not
578 functional in the TTX:PTX:Saline condition.

579 Collectively, our voltage clamp experiments indicated that there are graded
580 synapses, which are primarily ineffective in TTX:Saline, that are modulated to become
581 effective, or to become stronger (IC to LPG synapse), during Gly^1-SIFamide application.
582 In some modulatory conditions, graded transmission can be sufficient for CPG neurons
583 to generate coordinated network oscillations in the absence of spike-mediated
584 transmission (43, 46, 49). We tested whether graded transmission is also sufficient to
585 drive the Gly^1-SIFamide gastric mill rhythm in the absence of action potentials.

586 In normal saline conditions, recording from the neurons in current-clamp mode, only
587 the pyloric rhythm was active, with LPG and PD (*pdn* recording) generating pyloric-
588 timed bursting activity (Fig. 5A, left). During application of Gly^1-SIFamide (5 μM), there
589 was a coordinated gastric mill rhythm between LPG, LG, IC, and DG neurons (Fig. 5A,
590 right) (12, 21, 28). When spike-mediated transmission was blocked by eliminating action
591 potential generation with TTX (0.1 μM) (Fig. 5B), the neurons exhibited stable resting
592 membrane potentials without oscillations. However, during TTX plus Gly^1-SIFamide
593 application (5 μM), LPG, LG, IC, and DG generated coordinated gastric mill-timed
594 oscillations (Fig. 5B, right; n = 2). There was coordination of both pyloric (grey lines) and
595 gastric mill-timed (e.g., shaded box) oscillations between the neurons (Fig. 5B, right).
596 Inhibitory relationships are suggested, for example, in the most hyperpolarized
597 membrane potentials in DG occurring during the most depolarized membrane potentials
598 in LPG (Fig. 5B, dotted box). Thus, graded transmission was sufficient to mediate

599 coordinated gastric mill network activity in the Gly[1]-SIFamide modulatory state. These
600 experiments plus our previous study (21) demonstrated that LPG and the LG, IC, DG
601 group of gastric mill neurons contribute to coordination of gastric mill bursting in the
602 Gly[1]-SIFamide modulatory state.

603 Our voltage-clamp analysis focused on whether there was modulation of
604 bidirectional synapses between LPG and each of the other gastric mill neurons, as we
605 were particularly interested in how well the switching neuron LPG is integrated into the
606 gastric mill network in the Gly[1]-SIFamide modulatory condition. However, the triphasic
607 pattern of the Gly[1]-SIFamide gastric mill rhythm requires chemical synapses from some
608 or all of the LG, IC, and DG gastric mill neurons (21). Voltage-clamp analysis of all
609 synaptic combinations is a daunting task and we instead turned to entrainment
610 experiments to quantify the relative ability of each gastric mill neuron to regulate gastric
611 mill-timed activity of each of the other gastric mill neurons in the intact network.

612

613 Entrainment

614 To examine the ability of gastric mill neurons to regulate gastric mill bursting of
615 the other neurons, we injected rhythmic depolarizing current into each entraining neuron
616 (LG, IC, DG, or LPG [both copies]) across a range of burst frequencies (0.03 – 0.12 Hz;
617 see Methods) and quantified its ability to entrain the burst frequency of the other
618 neurons (Figs. 6 – 8; Supplemental Figs. S1 – S9).

619

620 LG entrainment of IC, DG, and LPG

621 We first examined whether LG could entrain IC, DG, and LPG neurons in Gly[1]-
622 SIFamide (5 μM, Fig. 6). In an example experiment, prior to any manipulations, LG was

623 bursting at approximately 0.03 Hz and IC, DG, and LPG were bursting in a relatively
624 coordinated manner (Fig. 6Ai-Ci, “No Entrainment”). For clarity, for all entrainment
625 frequencies presented, we use upward arrowheads to indicate the onset of each
626 entrained neuron burst and only show recordings of the test neurons. When LG was
627 stimulated with an entrainment frequency of 0.06 Hz (upward arrowheads), IC
628 generated a slow burst with each LG stimulation (Fig. 6Aii, boxes). As LG entrainment
629 frequency was increased, IC continued to generate 1-2 slow bursts within each LG
630 stimulation cycle, with two slow IC bursts triggered by an LG stimulation more frequently
631 at higher entrainment frequencies (Fig. 6Aii). IC bursts in both pyloric- and gastric mill-
632 time. IC gastric mill bursts were identified as previously described (Fig. 6Aii, boxes; see
633 Methods) (21). DG bursts overlapped with LG bursts in the No Entrainment condition,
634 except for one LG cycle, where DG burst twice within the cycle (Fig. 6Bi, No
635 Entrainment, dotted line). However, when the LG entrainment frequency was increased
636 from 0.06 Hz to 0.09 Hz, DG generated one burst for every two LG cycles (Fig. 6Bii). At
637 0.12 Hz entrainment frequency, DG burst frequency slowed further, such that DG
638 generated one burst for every four LG cycles (Fig. 6Bii). Thus, DG was coordinated with
639 LG at higher entrainment frequencies but not in a 1:1 relationship. Finally, for LG and
640 LPG slow bursting, without entrainment, LPG typically generated one burst per LG
641 cycle, except for one cycle where LPG generated two slow bursts (Fig. 6Ci, No
642 Entrainment). As the LG entrainment frequency was increased from 0.06 Hz to 0.12 Hz,
643 LPG appeared to maintain 1:1 coordinated slow bursting (Fig. 6Cii). At 0.12 Hz LG
644 entrainment frequency, a 1:1 relationship between LPG and LG persisted, although the
645 relative timing between each LPG burst and the onset of the LG bursts was less

646 consistent than at lower entrainment frequencies (Fig. 6Cii, 0.12Hz). LG does regulate
647 LPG slow burst cycle period (21). The example experiment shown indicates that LG
648 was able to entrain LPG within a range of frequencies (0.06 – 0.09 Hz), whereas above
649 that, LG regulated the LPG cycle period but was not able to entrain LPG bursting.
650 Across preparations, to determine whether IC, DG, and LPG neurons were
651 entrained to the LG entrainment frequencies, we plotted the instantaneous burst
652 frequencies (1/time between two consecutive bursts) against LG entrainment frequency
653 for all gastric mill-timed bursting, across all preparations (Fig. 6Aiii-Ciii). Each color
654 represents one preparation. For LG and IC, the data points from each preparation
655 clustered mostly on the solid diagonal line which indicates a 1:1 relationship of LG and
656 IC bursting (Fig. 6Aiii). For instance, at 0.06 Hz, 0.075 Hz, and 0.09 Hz there are a total
657 of 71, 48, and 71 cycles plotted, respectively. However, these data points are largely
658 overlapping due to their entrainment by LG at these frequencies (Fig. 6Aiii; n = 3 – 7
659 preparations per frequency; see Table 4 for numbers of cycles at each frequency). At
660 some frequencies, in some preparations, IC did not burst in a 1:1 manner, e.g., 0.06 Hz
661 and 0.12 Hz (Fig. 6Aiii). Diagonal lines indicate other modes of entrainment in which the
662 test neuron burst frequency was a multiple (or fraction) of the entrainment frequency
663 (Fig. 6Aiii, dashed diagonal lines, see Methods). The addition of these lines enabled us
664 to determine whether the data points not clustered on the 1:1 diagonal line were still
665 entrained to the LG frequency by clustering at another entrainment mode, or perhaps
666 not entrained if spread between entrainment modes. For instance, at 0.06 Hz, data
667 points for instantaneous IC burst frequencies clustered primarily near the 1:1 line (65/71
668 data points). However, the additional points fell near the 1:2 (2/71), 4:1 (1/71), or 5:1

669 (3/71) lines, indicating that even if it was not a 1:1 relationship for every IC burst, IC
670 activity was linked to that of LG and therefore was entrained by LG at 0.06 Hz.
671 Conversely, at 0.12 Hz, while some data points fell on integer lines, many fell between
672 them, indicating that IC was not readily entrained by LG at this frequency (Fig. 6Aiii).
673 For LG and DG, there was a range of instantaneous DG burst frequencies at
674 each LG entrainment frequency (Fig. 6Biii; n = 2-7, Table 4). Unlike IC, DG was not
675 locked to primarily one mode of entrainment. For example, in one preparation (Fig. 6Bii,
676 light blue data points), DG was entrained 1:1 at 0.05 Hz, but at other entrainment
677 frequencies DG exhibited a 1:2 (0.06 – 0.09 Hz) or 1:3 (0.09 – 0.12 Hz) relationship to
678 LG bursting. Overall, LG to DG entrainment appeared to be weaker than LG to IC, e.g.,
679 note the spread of points between entrainment lines for an entrainment frequency of
680 0.06 Hz (Fig. 6Biii). However, it was a relatively small number of points (7/35 data
681 points) that were spread between entrainment mode lines, the remainder of the data
682 points clustered near 1:1 (12/35 data points), 1:2 (10/35), and 1:3 (6/35) lines. Thus, LG
683 had some ability to entrain DG, although not always in a 1:1 relationship (Fig. 6Biii).
684 For LG and LPG slow bursting, we observed a range of instantaneous LPG slow
685 burst frequencies at most entrainment frequencies, except at 0.075 and 0.09 Hz (Fig.
686 6Ciii, n = 2-8, Table 4). Although some data points fell on entrainment mode lines, many
687 points, across multiple experiments, were spread between entrainment modes between
688 0.03 and 0.06 Hz, and for 0.12 Hz (Fig. 6Ciii). However, at 0.075 and 0.09 Hz, LPG data
689 points clustered on the 1:1 entrainment mode, with little variability, suggesting that LG
690 can entrain LPG within a limited frequency range (Fig. 6Ciii). While these plots enabled
691 a qualitative assessment of entrainment, we pursued a quantitative analysis as well.

692

693 Quantification of LG Entrainment of IC, DG, and LPG

694 To quantify entrainment between LG and IC, DG, and LPG, we collapsed the
695 data points at each entrainment frequency into a single value using a previously
696 described approach to quantify integer coupling relationships, e.g., 1:1, 2:1, etc., for
697 entrainment neuron/test neuron burst frequencies (35). Specifically, we first calculated
698 the ratio between each instantaneous neuron burst frequency and its respective LG
699 entrainment frequency and then used the significands (value to the right of the decimal)
700 from each set of ratios (i.e., IC/LG, DG/LG, LPG/LG) at each entrainment frequency to
701 generate a cumulative probability distribution (c.d.f.) of significands (Fig. 6D;
702 Supplemental Fig. S1). Perfect integer coupling would result in all significands being
703 close to 0 or 1. However, if there was no relationship between entrainment frequency
704 and test neuron burst frequency, then the significands would be distributed relatively
705 evenly between 0 and 1, resulting in a c.d.f. close to a diagonal line (y = x) (Fig. 6D, red
706 diagonal line) (35). For the example entrainment frequency of 0.06 Hz, c.d.f.s of
707 significands (bin size 0.01) for each of the test neurons are overlaid (Fig. 6D; IC, black;
708 DG, dark grey; LPG, light grey; remaining entrainment frequency c.d.f.s in Supplemental
709 Fig. S1). The blue dotted line indicates an extreme in which 50% of a theoretical
710 significand distribution is 0 and 50% is 1, indicating an example of perfect entrainment
711 (Fig. 6D, blue dotted line). In the c.d.f. for IC significands (black) ~70 % of significands
712 were less than ~0.1 (Fig. 6D, black shape). This shape reflects the clustering of IC
713 instantaneous burst frequency around 1:1 coupling at 0.06 Hz entrainment in the scatter
714 plot (Fig. 6Aiii). The c.d.f. of DG significands indicates that fewer were close to 0 or 1

715 (Fig. 6D, dark grey). This reflects the spread of some DG data points between
716 entrainment modes at 0.06 Hz in the scatter plot (Fig. 6Biii). The c.d.f. of LPG
717 significands indicated even weaker integer coupling at 0.06 Hz entrainment frequency,
718 with the distribution being more similar to the diagonal line, demonstrating a relatively
719 uniform distribution between 0 and 1 (Fig. 6D, light grey). This reflects the large spread
720 of LPG data points between entrainment modes at 0.06 Hz (Fig. 6Ciii). Qualitatively, the
721 c.d.f. histograms suggest that LG entrains IC more strongly than DG but does not
722 entrain LPG at 0.06 Hz (Fig. 6D). Consistent with the scatter plots (Fig. 6Ciii), the c.d.f.s
723 for LG to LPG entrainment at 0.075 and 0.09 indicate stronger integer coupling
724 (Supplemental Fig. S1).

725 Once the c.d.f. for each test neuron, at each entrainment frequency (Fig. 6D;
726 Supplemental Fig. S1), was determined, we calculated an overall measure of the extent
727 of integer coupling at each entrainment frequency by calculating the area between each
728 c.d.f. histogram (test neuron coupling) and the diagonal line (no integer coupling) (Fig.
729 6D, shaded regions). These area measurements for each neuron were plotted against
730 entrainment frequency, including from the example c.d.f.s for 0.06 Hz in figure 6D (Fig.
731 6E, downward arrow/dotted line). The dashed line at y = 0.25 indicates an example of
732 perfect integer coupling, where test neuron burst frequency is equal to the entrainment
733 neuron frequency, i.e., the area between the blue dotted line and the red diagonal line in
734 figure 6D (35). To determine whether the c.d.f. for each neuron at each entrainment
735 frequency was significantly different from a uniform distribution (i.e., the diagonal line),
736 we used a two-sample Kolmogorov-Smirnov test to compare each c.d.f. to a uniform
737 distribution. A corrected significance level of 0.007 (see Methods) for the comparison

738 between test neuron c.d.f. and a uniform distribution was used as the criterion for
739 entrainment at a particular frequency. Results of this statistical analysis is indicated
740 above each entrainment frequency for each neuron (Fig. 6E). For instance, the area
741 between the IC c.d.f. and the diagonal line at 0.03 Hz entrainment frequency was
742 approximately 0.45 but the IC c.d.f. area decreased at higher entrainment frequencies
743 (Fig. 6E, black line/symbols). Specifically, LG-to-IC integer coupling, and thus
744 entrainment, occurred between 0.03 – 0.09 Hz, but not at 0.12 Hz (Fig. 6E; Table 5).
745 Although the area between c.d.f. and the diagonal line for DG was greater at an
746 entrainment frequency of 0.05 and 0.075 Hz, than at other frequencies (Fig. 6E, dark
747 grey line/circles), DG was entrained by LG at all entrainment frequencies (Table 5).
748 Finally, the area for LPG was below 0.25 across frequencies but was non-zero (Fig. 6E,
749 light grey line/circles) and this area measurement was different from the uniform
750 distribution at all entrainment frequencies except 0.06 Hz (Table 5). Overall, these
751 results indicate that IC, DG, and LPG were integer coupled to and entrained by LG to
752 some extent, supporting our voltage-clamp analysis that there was a functional synapse
753 between these neurons in Gly^{1}-SIFamide.
754
755 <u>Entrainment and integer coupling among the other gastric mill neurons</u>
756 For the remainder of the neurons, we focused on the quantification afforded by
757 generating c.d.f.s of significands at each entrainment frequency, and measuring the
758 area between the test neuron c.d.f. and a uniform distribution (no coupling). The
759 complete assessment of the ability of IC, DG, and LPG to entrain the other neurons,
760 including individual data points as in figure 6 are provided in Supplemental Figs. S2-S9.

761 Overall, we found that all neurons (LG, IC, DG, LPG) could entrain all other neurons, at
762 least at some entrainment frequencies, however the extent of entrainment was variable
763 (Figs. 6 – 8, Supplemental Figs. S1 - S9).

764 At an example IC entrainment frequency of 0.06 Hz (additional c.d.f.s in
765 Supplemental Fig. S3), IC most effectively entrained LPG (Fig. 7Ai, black) with ~60% of
766 LPG/IC significands being less than 0.1 (Fig. 7Ai; n = 3-9, Table 4). The c.d.f.s for DG
767 (dark grey) and LG (light grey) were closer to the diagonal line, with ~25% and ~20% of
768 significands less than 0.1, respectively (Fig. 7Ai). The c.d.f. of significands for IC/LG
769 (Fig. 7Ai, light grey) was fairly close to the uniform distribution (red diagonal line). In
770 fact, using the c.d.f.s compared to a uniform distribution, IC entrained LG at 0.04, 0.06,
771 and 0.12 Hz, but not at 0.05, 0.075, or 0.09 Hz (Fig. 7Aii; Table 5). LG appeared better
772 able to entrain IC as the LG/IC area measurements were farther away from zero
773 (compare Fig. 6D and Fig. 7Aii). IC entrained DG from 0.04 – 0.12 Hz, but not at 0.03
774 Hz (Fig. 7Aii, dark grey circles and line; Table 5). Finally, LPG was entrained by IC at all
775 entrainment frequencies (Fig. 7Aii; Table 5; Supplemental Figs. S2-S3). Thus, LG, DG,
776 and LPG were all integer coupled to and entrained by IC at some entrainment
777 frequencies, also supporting the presence of functional synapses from IC to LG, DG,
778 and LPG in Gly^1-SIFamide.

779 The DG neuron is the most likely to be uncoordinated with the other gastric mill
780 neurons in the Gly^1-SIFamide gastric mill rhythm (21, 28). Despite this, stimulating DG
781 across a range of entrainment frequencies revealed some degree of control over the
782 burst frequency of the other neurons. For example, DG entrainment of LG and IC at an
783 entrainment frequency of 0.06 Hz, was evident in the ~75-80% of significands that were

784 less than 0.1 for LG and IC, while there were ~35% of significands less than 0.1 for LPG
785 (Fig. 7Bi, shaded regions, LG (black); IC (dark grey); LPG (light grey) (additional c.d.f.s
786 in Supplemental Fig. S5). The area between each c.d.f. and the diagonal line indicated
787 that integer coupling was variable for DG to LG (black), IC (dark grey), and LPG (light
788 grey) (Fig. 7Bii). LG and IC were entrained to DG at 0.03 and 0.05 – 0.12 Hz, but not
789 entrained at 0.04 Hz (Fig. 7Bii; Table 5). LPG was entrained by DG at 0.04 – 0.06 and
790 0.09 Hz, but not entrained at 0.03, 0.075, or 0.12 Hz entrainment frequencies (Fig. 7Bii,
791 Table 5; Supplemental Figs. S4-S5). The entrainment results correlate with the voltage-
792 clamp analysis in that the DG to LPG synapse was weaker and more variable than LG
793 or IC to LPG synapses (Figs. 2-4).

794 In the Gly^1-SIFamide modulatory state, LPG more strongly entrained the DG
795 neuron compared to IC and LG. In the c.d.f. histogram for DG at a 0.06 Hz entrainment
796 frequency, ~45% of significands were less than 0.1, and the area between DG c.d.f. and
797 the diagonal was 0.21 (Fig. 8Ai-ii, black shaded region and black data point at
798 downward arrow, respectively). Based on calculations of area between the c.d.f.s and
799 the diagonal line of no entrainment (Fig. 8Ai-ii; Supplemental Figs. S6-S7), LG was
800 entrained by LPG at 0.03, 0.075, and 0.09 Hz, but not at 0.04 – 0.06 or 0.12 Hz (Fig.
801 8Aii; Table 6). DG was entrained by LPG at all entrainment frequencies (Fig. 8Aii; Table
802 6) and IC was entrained by LPG only at 0.075 and 0.09 Hz, and not at the other
803 frequencies (Fig. 8Aii; Table 6; Supplemental Figs. S6-S7).

804 LPG can coordinate IC, LG, and DG during Gly^1-SIFamide application when all other
805 synapses are blocked. However, LPG was not necessary for coordinating these
806 neurons when other chemical synapses among the gastric mill neurons were intact (21),

807 suggesting overlapping functions of synaptic connections, which might interfere with
808 measurements of the ability of LPG to entrain the other neurons. Thus, we performed
809 an additional set of experiments to assess the ability of LPG to entrain LG, IC, and DG
810 neurons in the presence of Gly^1-SIFamide (SIF), plus picrotoxin (PTX, 10^{-5} M; Fig. 8Bi-
811 ii). As noted above, PTX application blocks glutamatergic inhibitory synapses, isolating
812 LPG from the glutamatergic LG, IC, and DG gastric mill neurons, but LPG cholinergic
813 transmission is not blocked by PTX (21, 30, 32, 50). Test neuron c.d.f.s in SIF:PTX (Fig.
814 8Bi) appeared larger than in Gly^1-SIFamide only (Fig. 8Ai). In SIF:PTX the c.d.f.
815 histograms for LG (dark grey), IC (light grey), and DG (black) had ~50-70% of
816 significands that were less than 0.1 at 0.06 Hz entrainment frequency (Fig. 8Bi, shaded
817 regions). Across all entrainment frequencies, most c.d.f.s appeared to indicate greater
818 entrainment in SIF:PTX compared to Gly^1-SIFamide alone (Supplemental Figs. S7 vs.
819 S9). Quantitatively, with glutamatergic synapses blocked (SIF:PTX), LPG entrained DG
820 between 0.04 – 0.12 Hz, but not at 0.03 Hz (Fig. 8Bii; Table 6). LPG was already able to
821 entrain DG from 0.04 – 0.12 Hz in Gly^1-SIFamide (Fig. 8Aii), but data was not obtained
822 at 0.03 Hz in this condition. However, for LG and IC, which were entrained by LPG from
823 0.04 – 0.12 Hz in Gly^1-SIFamide (Fig. 8Aii), in SIF:PTX LPG entrained them at all
824 frequencies (Fig. 8Bii, LG, dark grey line/circles; IC, light grey line/circles) (Fig. 8Bii;
825 Table 6; Supplemental Figs. S8-S9). Thus, it appears likely that synaptic actions from
826 LG, IC, and/or DG in Gly^1-SIFamide interfere with the ability of LPG to control LG and IC
827 bursting. Because only cholinergic LPG synapses were active in SIF:PTX, our
828 entrainment assay indicates direct functional synapses from LPG onto LG, IC, and DG

829 neurons in the Gly[1]-SIFamide modulatory state, in alignment with our voltage-clamp
830 findings (Figs. 2-4).
831
832 **Discussion**
833 In this study we determined that there are functional, bidirectional synapses between
834 LPG and gastric mill network neurons LG, IC, and DG in the modulatory state elicited by
835 the neuropeptide Gly[1]-SIFamide. As revealed by two electrode voltage-clamp
836 recordings, most of the synaptic connections are ineffective in saline conditions, but are
837 enhanced by Gly[1]-SIFamide (Fig. 9). Additionally, we found that each neuron, including
838 the switching neuron LPG, is capable of entraining other neurons in the network, within
839 a physiological frequency range during the Gly[1]-SIFamide modulatory state. Thus, in
840 addition to modulating intrinsic properties of LPG, thereby enabling dual frequency
841 oscillations (21, 22), the neuropeptide Gly[1]-SIFamide enables previously ineffective
842 synapses to become a functional pathway for a switching neuron to both be influenced
843 by, and to influence, neurons in a network to which it transiently belongs.
844
845 Modulation of Internetwork Synapses
846 Neuromodulator regulation of synaptic strength contributes to CPG flexibility (39,
847 51). In particular, neuropeptide modulation of synapses occurs throughout nervous
848 systems with both pre- and postsynaptic sites of action (52–57). Modulator-elicited
849 enhancement of internetwork synapses can serve as the sole mechanism by which a
850 neuron is both recruited to generate activity at a second frequency, and coordinated
851 with other neurons (6, 8, 20). In the saline state, LPG activity is pyloric due to electrical

852 coupling with the pyloric pacemaker ensemble (12, 58). Gly^1-SIFamide modulates
853 multiple ionic currents to switch LPG into dual pyloric and gastric mill-timed bursting (12,
854 22). However, we found that in saline, among gastric mill neurons and LPG, there was
855 only a weak synapse from IC onto LPG. Thus, modulation of intrinsic properties is not
856 sufficient to coordinate LPG with other gastric mill neurons. The ability of Gly^1-SIFamide
857 to also enhance inhibitory connections between LPG and gastric mill neurons LG, IC,
858 and DG, explain the ability of LPG and LG, IC, and DG to entrain each other (this study)
859 and to generate a coordinated rhythm (21, 28), despite being functionally disconnected
860 in saline conditions (Fig. 9A). Thus, parallel modulatory actions impact a switching
861 neuron such that (1) modulation of intrinsic properties enables generation of rhythmic
862 activity at a second frequency, and (2) modulation of synaptic properties between
863 switching and network neurons enables coordination within the second network.
864 Regardless of whether synaptic modulation occurs in isolation or with modulation
865 of intrinsic properties, network output is determined by complex interactions between
866 both sets of properties (59). Such interactions may explain the diversity of entrainment
867 we observed. Most simply, entrainment is 1:1 coordination between two neurons or
868 rhythmic patterns, with test neuron frequency equal to entrainment frequency (60–63).
869 While 1:1 entrainment among LPG, LG, IC, and DG occurred (notably from LG to IC),
870 we also observed other coordination patterns. For instance, regardless of the
871 entrainment neuron, DG exhibited some 1:2 entrainment (one DG burst for every two
872 entrainment neuron bursts). In addition to LPG, DG is an endogenous burster in Gly^1-
873 SIFamide (21). Slower DG bursting at higher entrainment frequencies suggests that
874 rhythmic synaptic inhibition may not be able to overcome the slower ionic currents

875 underlying endogenous DG bursting, reinforcing the combined contributions of synaptic
876 and intrinsic properties to network output.

877 Although communication was bidirectional between all pairs, differences in
878 synaptic properties were observed. For example, LPG cholinergic output synapses onto
879 the gastric mill neurons have a slower time course than glutamatergic synapses onto
880 LPG, as do cholinergic versus glutamatergic synapses within the pyloric network (47,
881 48). Pharmacological block of glutamatergic transmission makes it likely that the LPG to
882 DG synapse is direct. However, determining direct connections is difficult, even in small
883 networks due to the complicating factor of highly prevalent electrical coupling, common
884 across networks (64–66). For example, LPG-elicited synaptic currents in LG and IC are
885 difficult to interpret due to LG/IC electrical coupling. Identifying direct synapses among
886 gastric mill neurons would require photoinactivation to selectively eliminate subsets of
887 neurons (47).

888 In addition to chemical synapses, properties of electrical synapses among gastric
889 mill neurons are likely important in the Gly^1-SIFamide rhythm. During Gly^1-SIFamide,
890 LG/IC gastric mill-timed bursting is typically coincident (21), likely due to electrical
891 coupling (64). However, while LG entrained IC in a mostly 1:1 fashion across most
892 frequencies, IC only entrained LG at half of the frequencies. We speculate this
893 difference is due to either rectifying electrical coupling, where positive current flows
894 better from LG to IC, or an inhibitory synapse from IC to LG (67) that is stronger than
895 LG/IC electrical coupling. Rectification promotes CPG flexibility by enabling differential
896 modulatory actions on coupled neurons, and may be important for neuronal switching
897 between networks (11, 68–70). For instance, rectifying LPG/PD electrical coupling (58)

898 may be important for enabling LPG switching into gastric mill timing (S-RH Fahoum, F
899 Nadim, and DM Blitz, unpublished observations). Similarly, LG/IC rectification could
900 enable IC recruitment from pyloric-only to dual pyloric/gastric mill timing, while
901 preventing LG from being pulled into pyloric-timed activity. Thus, rectification can play
902 an important role in maintaining network distinctions, even as some neurons are
903 recruited to participate in secondary networks.
904

905 Functional Implications of Synaptic Modulation

906 Synaptic modulation is a common mechanism for regulating the relative timing of
907 neurons, and thus the particular activity pattern, although modulation of ionic currents
908 that alter responses to synaptic input can also be important for patterning network
909 output (1, 59, 71, 72). Other gastric mill rhythm versions are biphasic (73–75), whereas
910 the Gly^1-SIFamide-elicited rhythm has a third phase, during which endogenous LPG
911 slow bursting is out of phase with the other neurons ((21). Inhibitory synapses from LPG
912 to LG, IC, and DG likely ensure the offset between LPG and the other neurons, while
913 synapses between LG, IC, and DG (Fig. 9B) are likely important for maintaining offsets
914 in their timing. In fact, the rhythm collapses into two phases (LG/IC/DG co-active and
915 alternating with LPG) when glutamatergic synapses are blocked via PTX, leaving only
916 cholinergic LPG synapses functional (21). Additionally, LPG regulates LG and DG
917 neuron firing frequency in Gly^1-SIFamide (21). Collectively, these results emphasize the
918 full incorporation of an endogenously bursting switching neuron, such that it can
919 contribute to pattern generation in a second network.

920 Spike-mediated and graded neurotransmission play complementary roles at
921 vertebrate and invertebrate synapses and are both subject to neuromodulation (55, 76–
922 81). In the STNS, spike-mediated and graded transmission occur, but graded
923 transmission is dominant and can be sufficient to generate fully coordinated pyloric
924 rhythms under some modulatory states (43, 44, 46). Here we determined that a
925 coordinated gastric mill rhythm can occur without spike-mediated transmission in the
926 Gly^1-SIFamide state. However, whether rhythm generating mechanisms differ for Gly^1-
927 SIFamide compared to other gastric-mill rhythm activators, and whether they require
928 spike-mediated transmission is unknown (75, 82). Rhythm generation of episodic
929 behaviors (e.g., chewing, locomotion) typically relies on intra-network synapses, as
930 opposed to pacemaker neurons generating continuously active rhythms (e.g., pyloric,
931 respiratory) (1, 83). In other gastric mill rhythm versions, reciprocal inhibition between
932 the LG and Int1 neurons forms the core rhythm generator. Gly^1-SIFamide elicits
933 endogenous bursting in LPG and DG, but IC and LG cannot generate rhythmic activity
934 in the absence of chemical synapses in Gly^1-SIFamide (12, 21, 22). Thus, in addition to
935 coordinating endogenous oscillations of the LPG switching neuron plus DG with other
936 network neurons, the modulated graded synapses are likely necessary for rhythmic
937 activity in at least some of the network neurons.
938

939 Conclusions

940 There is increasing evidence from small- to large-scale, and local to long-
941 distance, that neuromodulators can rapidly alter network composition based on sensory
942 information, a required behavior, or required coordination between multiple behaviors

943 (14–17, 19, 84–86). Our results indicate that parallel modulation of intrinsic and synaptic
944 properties of a switching neuron can mediate recruiting a neuron into generating
945 rhythmic activity at a second frequency (intrinsic properties) and coordinating those
946 oscillations with other neurons in the network (synaptic properties), potentially providing
947 additional flexibility under different behavioral states. It is also possible that the
948 combined influence of parallel actions is necessary based on the particular complement
949 of intrinsic and synaptic properties that must be overcome for a switching neuron to
950 "escape" from its home network.
951

952 **SUPPLEMENTAL MATERIAL**

953 Supplemental Figs. S1–S9:
954 https://figshare.com/articles/figure/Supplemental_Synapses_pdf/25559007

References

1. **Bucher D**, **Haspel G**, **Golowasch J**, **Nadim F**. Central pattern generators. In: *eLS*. John Wiley & Sons, Ltd: Chichester, 2015.

2. **Grillner S**, **Kozlov A**. The cpgs for limbed locomotion–facts and fiction. *Intern J of Molec Sci* 22, 2021. doi: 10.3390/ijms22115882.

3. **Leiras R**, **Cregg JM**, **Kiehn O**. Brainstem circuits for locomotion. *Ann Rev Neurosci* 45: 63–85, 2022. doi: 10.1146/ANNUREV-NEURO-082321-025137.

4. **Doi A**, **Ramirez JM**. Neuromodulation and the orchestration of the respiratory rhythm. *Respir Physiol Neurobiol* 164: 96–104, 2008. doi: 10.1016/J.RESP.2008.06.007.

5. **Devineni A V.**, **Scaplen KM**. Neural circuits underlying behavioral flexibility: Insights from Drosophila. *Front Behav Neurosci* 15, 2022. doi: 10.3389/FNBEH.2021.821680.

6. **Hooper SL**, **Moulins M**. Cellular and synaptic mechanisms responsible for a long-lasting restructuring of the lobster pyloric network. *J Neurophysiol* 64: 1574, 1990. doi: 10.1152/jn.1990.64.5.1574.

7. **Weimann JM**, **Meyrand P**, **Marder E**. Neurons that form multiple pattern generators: Identification and multiple activity patterns of gastric/pyloric neurons in the crab stomatogastric system. *J Neurophysiol* 65: 111–122, 1991. doi: 10.1152/jn.1991.65.1.111.

8. **Meyrand P**, **Simmers J**, **Moulins M**. Dynamic construction of a neural network from multiple pattern generators in the lobster stomatogastric nervous system. *J Neurosci* 14: 630–644, 1994.

9. **Dickinson PS**. Interactions among neural networks for behavior. *Curr Opin Neurobiol* 5: 792–798, 1995. doi: 10.1016/0959-4388(95)80108-1.

10. **Tryba AK**, **Peña F**, **Lieske SP**, **Viemari J-C**, **Thoby-Brisson M**, **Ramirez J-M**. Differential modulation of neural network and pacemaker activity underlying eupnea and sigh-breathing activities. *J Neurophysiol* 99: 2114–2125, 2008. doi: 10.1152/jn.01192.2007.

11. **Drion G**, **Franci A**, **Sepulchre R**. Cellular switches orchestrate rhythmic circuits. *Biol Cybern* 113: 71–82, 2019. doi: 10.1007/s00422-018-0778-6.

12. **Fahoum S-RH**, **Blitz DM**. Neuronal switching between single- and dual-network activity via modulation of intrinsic membrane properties. *J Neurosci* 41: 7848–7863, 2021. doi: 10.1523/JNEUROSCI.0286-21.2021.

13. **Buzsáki G**, **Draguhn A**. Neuronal oscillations in cortical networks. *Science* 304: 1926–1930, 2004.

14. **Bouret S**, **Sara SJ**. Network reset: a simplified overarching theory of locus coeruleus noradrenaline function. *TINS* 28: 574–582, 2005. doi: 10.1016/J.TINS.2005.09.002.

15. **Kopell NJ**, **Gritton HJ**, **Whittington MA**, **Kramer MA**. Beyond the connectome: The dynome. *Neuron* 83: 1319–1328, 2014. doi: 10.1016/j.neuron.2014.08.016.

16. **Rangel LM**, **Rueckemann JW**, **Riviere PD**, **Keefe KR**, **Porter BS**, **Heimbuch IS**, **Budlong CH**, **Eichenbaum H**. Rhythmic coordination of hippocampal neurons during associative memory processing. *Elife* 5: 1–24, 2016. doi: 10.7554/eLife.09849.

17. **van den Brink RL**, **Pfeffer T**, **Donner TH**. Brainstem Modulation of Large-Scale Intrinsic Cortical Activity Correlations. *Front Hum Neurosci* 13, 2019. doi: 10.3389/FNHUM.2019.00340.

18. **Higley MJ**, **Cardin JA**. Spatiotemporal dynamics in large-scale cortical networks. *Curr Opin Neurobiol* 77: 1–7, 2022. doi: 10.1016/j.conb.2022.102627.

19. **Lohani S**, **Moberly AH**, **Benisty H**, **Landa B**, **Jing M**, **Li Y**, **Higley MJ**, **Cardin JA**. Spatiotemporally heterogeneous coordination of cholinergic and neocortical activity. *Nat Neurosci* 25: 1706–1713, 2022. doi: 10.1038/s41593-022-01202-6.

20. **Dickinson PS**, **Mecsas C**, **Marder E**. Neuropeptide fusion of two motor-pattern generator circuits. *Nature* 344: 155–158, 1990. doi: 10.1038/344155A0.

21. **Fahoum S-RH**, **Blitz DM**. Switching neuron contributions to second network activity. *J Neurophysiol* 131: 417–434, 2024. doi: 10.1152/JN.00373.2023.

22. **Snyder RR**, **Blitz DM**. Multiple intrinsic membrane properties are modulated in a switch from single- to dual-network activity. *J Neurophysiol* 128: 1181–1198, 2022. doi: 10.1152/JN.00337.2022.

23. **Gutierrez GJ**, **Grashow RG**. *Cancer borealis* stomatogastric nervous system dissection. *J Vis Exp* 23: 1–5, 2009. doi: 10.3791/1207.

24. **Hooper SL**, **Thuma JB**, **Guschlbauer C**, **Schmidt J**, **Büschges A**. Cell dialysis by sharp electrodes can cause nonphysiological changes in neuron properties. *J Neurophysiol* 114: 1255–1271, 2015. doi: 10.1152/jn.01010.2014.

25. **Huybrechts J**, **Nusbaum MP**, **Bosch L Vanden**, **Baggerman G**, **De Loof A**, **Schoofs L**. Neuropeptidomic analysis of the brain and thoracic ganglion from the Jonah crab, *Cancer borealis*. *Biochem Biophys Res Commun* 308: 535–544, 2003. doi: 10.1016/S0006-291X(03)01426-8.

26. **Yasuda A**, **Yasuda-Kamatani Y**, **Nozaki M**, **Nakajima T**. Identification of GYRKPPFNGSIFamide (crustacean-SIFamide) in the crayfish *Procambarus clarkii* by topological mass spectrometry analysis. *Gen and Comp Endocrinol* 135: 391–400, 2004. doi: 10.1016/j.ygcen.2003.10.001.

1028 27. **Dickinson PS**, **Stemmler EA**, **Cashman CR**, **Brennan HR**, **Dennison B**, **Huber**
1029 **KE**, **Peguero B**, **Rabacal W**, **Goiney CC**, **Smith CM**, **Towle DW**, **Christie AE**.
1030 SIFamide peptides in clawed lobsters and freshwater crayfish (Crustacea,
1031 Decapoda, Astacidea): A combined molecular, mass spectrometric and
1032 electrophysiological investigation. *Gen and Comp Endocrinol* 156: 347–360,
1033 2008. doi: 10.1016/j.ygcen.2008.01.011.

1034 28. **Blitz DM**, **Christie AE**, **Cook AP**, **Dickinson PS**, **Nusbaum MP**. Similarities and
1035 differences in circuit responses to applied Gly^1-SIFamide and peptidergic (Gly^1 -
1036 SIFamide) neuron stimulation. *J Neurophysiol* 121: 950–972, 2019. doi:
1037 10.1152/jn.00567.2018.

1038 29. **Schneider AC**, **Fox D**, **Itani O**, **Golowasch J**, **Bucher D**, **Nadim F**. Frequency-
1039 dependent action of neuromodulation. *eNeuro* 8, 2021. doi:
1040 10.1523/ENEURO.0338-21.2021.

1041 30. **Marder E**. Acetylcholine as an excitatory neuromuscular transmitter in the
1042 stomatogastric system of lobster. *Nature* 251: 730–731, 1974.

1043 31. **Marder E**. Cholinergic motor neurones in the stomatogastric system of the
1044 lobster. *J Physiol* 257: 63–86, 1976. doi: 10.1113/jphysiol.1976.sp011356.

1045 32. **Hooper SL**, **O'Neil MB**, **Wagner R**, **Ewer J**, **Golowasch J**, **Marder E**. The
1046 innervation of the pyloric region of the crab, Cancer borealis: homologous
1047 muscles in decapod species are differently innervated. *J Comp Physiol A* 159:
1048 227–240, 1986. doi: 10.1007/BF00612305.

1049 33. **Martinez D**, **Santin JM**, **Schulz D**, **Nadim F**. The differential contribution of
1050 pacemaker neurons to synaptic transmission in the pyloric network of the Jonah
1051 crab, *Cancer borealis*. *J Neurophysiol* 122: 1623–1633, 2019. doi:
1052 10.1152/jn.00038.2019.

1053 34. **Bucher D**, **Taylor AL**, **Marder E**. Central pattern generating neurons
1054 simultaneously express fast and slow rhythmic activities in the stomatogastric
1055 ganglion. *J Neurophysiol* 95: 3617–3632, 2006. doi: 10.1152/jn.00004.2006.

1056 35. **Powell D**, **Haddad SA**, **Gorur-Shandilya S**, **Marder E**. Coupling between fast
1057 and slow oscillator circuits in *Cancer borealis* is temperature-compensated. *Elife*
1058 10: e60454, 2021. doi: 10.7554/eLife.60454.

1059 36. **Nusbaum MP**, **Beenhakker MP**. A small-systems approach to motor pattern
1060 generation. *Nature* 417: 343–350, 2002. doi: 10.1038/417343a.

1061 37. **Daur N**, **Nadim F**, **Bucher D**. The complexity of small circuits: the stomatogastric
1062 nervous system. *Curr Opin Neurobiol* 41: 1–7, 2016. doi:
1063 10.1016/J.CONB.2016.07.005.

1064 38. **Blitz DM**. Neural circuit regulation by identified modulatory projection neurons.
1065 *Front Neurosci* 17, 2023. doi: 10.3389/FNINS.2023.1154769.

1066 39. **Nadim F**, **Bucher D**. Neuromodulation of neurons and synapses. *Curr Opin*
1067 *Neurobiol* 29: 48–56, 2014. doi: 10.1016/j.conb.2014.05.003.

1068 40. **Stein W**. Modulation of stomatogastric rhythms. *J Comp Physiol* 195: 989–1009,
1069 2009. doi: 10.1007/S00359-009-0483-Y.

1070 41. **Norris BJ**, **Coleman MJ**, **Nusbaum MP**. Pyloric motor pattern modification by a
1071 newly identified projection neuron in the crab stomatogastric nervous system. *J*
1072 *Neurophysiol* 75: 97–108, 1996. doi: 10.1152/JN.1996.75.1.97.

1073 42. **Marder E**, **Bucher D**. Understanding circuit dynamics using the stomatogastric
1074 nervous system of lobsters and crabs. *Ann Rev Physiol* 69: 291–316, 2007. doi:
1075 10.1146/annurev.physiol.69.031905.161516.

1076 43. **Raper JA**. Nonimpulse-mediated synaptic transmission during the generation of a
1077 cyclic motor program. *Science* 205: 304–306, 1979. doi: 10.1126/science.221982.

1078 44. **Graubard K**, **Raper JA**, **Hartline DK**. Graded synaptic transmission between
1079 spiking neurons. *PNAS* 77: 3733–3735, 1980.

1080 45. **Thirumalai V**, **Prinz AA**, **Johnson CD**, **Marder E**. Red pigment concentrating
1081 hormone strongly enhances the strength of the feedback to the pyloric rhythm
1082 oscillator but has little effect on pyloric rhythm period. *J Neurophysiol* 95: 1762–
1083 1770, 2006. doi: 10.1152/jn.00764.2005.

1084 46. **Rosenbaum P**, **Marder E**. Graded transmission without action potentials sustains
1085 rhythmic activity in some but not all modulators that activate the same current. *J*
1086 *Neurosci* 38: 8976–8988, 2018. doi: 10.1523/JNEUROSCI.2632-17.2018.

1087 47. **Eisen JS**, **Marder E**. Mechanisms underlying pattern generation in lobster
1088 stomatogastric ganglion as determined by selective inactivation of identified
1089 neurons. III. Synaptic connections of electrically coupled pyloric neurons. *J*
1090 *Neurophysiol* 48: 1392–1415, 1982. doi: 10.1152/jn.1982.48.6.1392.

1091 48. **Marder E**, **Eisen JS**. Transmitter identification of pyloric neurons: electrically
1092 coupled neurons use different transmitters. *J Neurophysiol* 51: 1345–1361, 1984.

1093 49. **Harris-Warrick RM**, **Flamm RE**. Multiple mechanisms of bursting in a conditional
1094 bursting neuron. *J Neurosci* 7: 2113–2128, 1987. doi: 10.1523/jneurosci.07-07-
1095 02113.1987.

1096 50. **Bidaut M**. Pharmacological dissection of pyloric network of the lobster
1097 stomatogastric ganglion using picrotoxin. *J Neurophysiol* 44: 1089–1101, 1980.
1098 doi: 10.1152/jn.1980.44.6.1089.

1099 51. **Marder E**, **Thirumalai V**. Cellular, synaptic and network effects of
1100 neuromodulation. *Neural Networks* 15: 479–493, 2002. doi: 10.1016/S0893-
1101 6080(02)00043-6.

1102 52. **Merighi A**, **Salio C**, **Ferrini F**, **Lossi L**. Neuromodulatory function of
1103 neuropeptides in the normal CNS. *J Chem Neuroanat* 42: 276–287, 2011. doi:
1104 10.1016/J.JCHEMNEU.2011.02.001.

1105 53. **Bacci A**, **Huguenard JR**, **Prince DA**. Differential modulation of synaptic
1106 transmission by neuropeptide Y in rat neocortical neurons. *Proc Natl Acad Sci U*
1107 *S A* 99: 17125–17130, 2002. doi: 10.1073/PNAS.012481899.

1108 54. **Ormerod KG**, **Jung JH**, **Mercier AJ**. Modulation of neuromuscular synapses and
1109 contraction in Drosophila 3rd instar larvae. *J Neurogenet* 32: 183–194, 2018. doi:
1110 10.1080/01677063.2018.1502761.

1111 55. **Zhao S**, **Sheibanie AF**, **Oh M**, **Rabbah P**, **Nadim F**. Peptide neuromodulation of
1112 synaptic dynamics in an oscillatory network. *J Neurosci* 31: 13991–14004, 2011.
1113 doi: 10.1523/JNEUROSCI.3624-11.2011.

1114 56. **Nusbaum MP**, **Blitz DM**, **Marder E**. Functional consequences of neuropeptide
1115 and small-molecule co-transmission HHS Public Access. *Nat Rev Neurosci* 18:
1116 389–403, 2017. doi: 10.1038/nrn.2017.56.

1117 57. **Koh HY**, **Vilim FS**, **Jing J**, **Weiss KR**. Two neuropeptides colocalized in a
1118 command-like neuron use distinct mechanisms to enhance its fast synaptic
1119 connection. *J Neurophysiol* 90: 2074–2079, 2003. doi: 10.1152/JN.00358.2003.

1120 58. **Shruti S**, **Schulz DJ**, **Lett KM**, **Marder E**. Electrical coupling and innexin
1121 expression in the stomatogastric ganglion of the crab *Cancer borealis*. *J*
1122 *Neurophysiol* 112: 2946–2958, 2014. doi: 10.1152/jn.00536.2014.

1123 59. **Marder E**, **Calabrese RL**. Principles of rhythmic motor pattern generation. *Physiol*
1124 *Rev* 76: 687–717, 1996. doi: 10.1152/physrev.1996.76.3.687.

1125 60. **Weimann JM**, **Skiebe P**, **Heinzel HG**, **Soto C**, **Kopell N**, **Jorge-Rivera JC**,
1126 **Marder E**. Modulation of oscillator interactions in the crab stomatogastric ganglion
1127 by crustacean cardioactive peptide. *J Neurosci* 17: 1748–1760, 1997. doi:
1128 10.1523/JNEUROSCI.17-05-01748.1997.

1129 61. **Kawahara K**, **Kumagai S**, **Nakazono Y**, **Miyamoto Y**. Coupling between
1130 respiratory and stepping rhythms during locomotion in decerebrate cats. *J Appl*
1131 *Physiol* 67: 110–115, 1989. doi: 10.1152/jappl.1989.67.1.110.

1132 62. **Maezawa H**, **Koganemaru S**, **Matsuhashi M**, **Hirata M**, **Funahashi M**, **Mima T**.
1133 Entrainment of chewing rhythm by gait speed during treadmill walking in humans.
1134 *Neurosci Res* 156: 88–94, 2020. doi: 10.1016/J.NEURES.2020.02.008.

1135 63. **Bartos M**, **Manor Y**, **Nadim F**, **Marder E**, **Nusbaum MP**. Coordination of fast and
1136 slow rhythmic neuronal circuits. *J Neurosci* 19: 6650–6660, 1999. doi:
1137 10.1523/JNEUROSCI.19-15-06650.1999.

1138 64. **Marder E**, **Gutierrez GJ**, **Nusbaum MP**. Complicating connectomes: Electrical
1139 coupling creates parallel pathways and degenerate circuit mechanisms. *Dev*
1140 *Neurobiol* 77: 597–609, 2017. doi: 10.1002/DNEU.22410.

1141 65. **Nadim F**, **Li X**, **Gray M**, **Golowasch J**. The role of electrical coupling in rhythm
1142 generation in small networks. In: *Network Functions and Plasticity: Perspectives*
1143 *from Studying Neuronal Electrical Coupling in Microcircuits*. 2017, p. 51–78.

1144 66. **Connors BW**. Synchrony and so much more: Diverse roles for electrical
1145 synapses in neural circuits. *Dev Neurobiol* 77: 610–624, 2017. doi:
1146 10.1002/dneu.22493.

1147 67. **Weimann JM**, **Marder E**. Switching neurons are integral members of multiple
1148 oscillatory networks. *Curr Biol* 4: 896–902, 1994. doi: 10.1016/S0960-
1149 9822(00)00199-8.

1150 68. **Gutierrez GJ**, **Marder E**. Rectifying electrical synapses can affect the influence of
1151 synaptic modulation on output pattern robustness. *J Neurosci* 33: 13238–13248,
1152 2013. doi: 10.1523/JNEUROSCI.0937-13.2013.

1153 69. **Gutierrez GJ**, **O'Leary T**, **Marder E**. Multiple mechanisms switch an electrically
1154 coupled, synaptically inhibited neuron between competing rhythmic oscillators.
1155 *Neuron* 77: 845–858, 2013. doi: 10.1016/j.neuron.2013.01.016.

1156 70. **Palacios-Prado N**, **Huetteroth W**, **Pereda AE**. Hemichannel composition and
1157 electrical synaptic transmission: molecular diversity and its implications for
1158 electrical rectification. *Front Cell Neurosci* 8: 324, 2014. doi:
1159 10.3389/FNCEL.2014.00324.

1160 71. **Katz PS**. Evolution of central pattern generators and rhythmic behaviours.
1161 *Philosoph Trans* 371, 2016. doi: 10.1098/rstb.2015.0057.

1162 72. **Stein P**. Central pattern generators in the turtle spinal cord: selection among the
1163 forms of motor behaviors. *J Neurophysiol* 119: 422–440, 2018. doi:
1164 10.1152/jn.00602.2017.

1165 73. **Christie AE**, **Stein W**, **Quinlan JE**, **Beenhakker MP**, **Marder E**, **Nusbaum MP**.
1166 Actions of a histaminergic/peptidergic projection neuron on rhythmic motor
1167 patterns in the stomatogastric nervous system of the crab *Cancer borealis*. *J*
1168 *Comp Neurol* 469: 153–169, 2004. doi: 10.1002/CNE.11003.

1169 74. **Blitz DM**, **Beenhakker MP**, **Nusbaum MP**. Different sensory systems share
1170 projection neurons but elicit distinct motor patterns. *J Neurosci* 24: 11381–11390,
1171 2004. doi: 10.1523/JNEUROSCI.3219-04.2004.

1172 75. **White RS**, **Nusbaum MP**. The same core rhythm generator underlies different
1173 rhythmic motor patterns. *J Neurosci* 31: 11484–11494, 2011. doi:
1174 10.1523/JNEUROSCI.1885-11.2011.

76. **Johnson BR**, **Harris-Warrick RM**. Aminergic modulation of graded synaptic transmission in the lobster stomatogastric ganglion. *J Neurosci* 10: 2066–2076, 1990. doi: 10.1523/jneurosci.10-07-02066.1990.

77. **DiCaprio RA**. Nonspiking and spiking proprioceptors in the crab: Nonlinear analysis of nonspiking TCMRO afferents. *J Neurophysiol* 89: 1826–1836, 2003. doi: 10.1152/jn.00978.2002.

78. **Alle H**, **Geiger JRP**. Combined analog and action potential coding in hippocampal mossy fibers. *Science* 311: 1290–1293, 2006. doi: 10.1126/science.1119055.

79. **Shu Y**, **Hasenstaub A**, **Duque A**, **Yu Y**, **McCormick DA**. Modulation of intracortical synaptic potentials by presynaptic somatic membrane potential. *Nature* 441: 761–765, 2006. doi: 10.1038/nature04720.

80. **Beckers U**, **Egelhaaf M**, **Kurtz R**. Precise timing in fly motion vision is mediated by fast components of combined graded and spike signals. *Neuroscience* 160: 639–650, 2009. doi: 10.1016/j.neuroscience.2009.02.045.

81. **Ivanov AI**, **Calabrese RL**. Spike-mediated and graded inhibitory synaptic transmission between leech interneurons: Evidence for shared release sites. *J Neurophysiol* 96: 235–251, 2006. doi: 10.1152/jn.01094.2005.

82. **Coleman MJ**, **Meyrand P**, **Nusbaum MP**. A switch between two modes of synaptic transmission mediated by presynaptic inhibition. *Nature* 378: 502–505, 1995. doi: 10.1038/378502a0.

83. **Grillner S**, **El Manira A**. Current principles of motor control, with special reference to vertebrate locomotion. *Physiol Rev* 100: 271–320, 2020. doi: 10.1152/physrev.00015.2019.

84. **Bartlett D**, **Leiter JC**. Coordination of breathing with nonrespiratory activities. *Comp Physiol* 2: 1387–1415, 2012.

85. **Roopun AK**, **Kramer MA**, **Carracedo LM**, **Kaiser M**, **Davies CH**, **Traub RD**, **Kopell NJ**, **Whittington MA**. Period concatenation underlies interactions between gamma and beta rhythms in neocortex. *Front Cell Neurosci* 2: 1–8, 2008. doi: 10.3389/neuro.03.001.2008.

86. **Martin C**, **Ravel N**. Beta and gamma oscillatory activities associated with olfactory memory tasks: different rhythms for different functional networks? *Front Behav Neurosci* 8, 2014. doi: 10.3389/FNBEH.2014.00218.

1210 **Figure Legends**
1211

1212 **Figure 1. STNS schematic and circuit diagram of pyloric and gastric mill**
1213 **networks.**

1214 ***A,*** The modulatory projection neuron 5 (MCN5; two copies) has a soma (arrow) in each
1215 commissural ganglion (CoG) of the stomatogastric nervous system (STNS). The axon of
1216 each MCN5 neuron projects through the inferior oesophageal (*ion*), oesophageal (*on*),
1217 and stomatogastric (*stn*) nerves and terminates in the stomatogastric ganglion (STG) to
1218 synapse with motor neurons and interneurons responsible for generating rhythmic
1219 activity of the pyloric (~1 Hz, food filtering) and gastric mill (~0.1 Hz, food chewing)
1220 feeding-related behaviors. Each pyloric and gastric mill motor neuron has axons that
1221 project through posterior motor nerves to innervate muscles that control the movements
1222 for pyloric and gastric mill activity. Vaseline wells (*circles*) were built around motor
1223 nerves to record extracellular activity of these neurons. ***B,*** The circuit diagram of the
1224 STG indicates known electrical (*resistor and diode symbols*) and inhibitory chemical
1225 (*ball and stick*) synapses among pyloric and gastric mill neurons in saline conditions.
1226 When active, the MCN5 neuron targets both pyloric and gastric mill neurons (*grey*
1227 *boxes*), however, synaptic modulation targets of MCN5 are unknown. Abbreviations,
1228 Ganglia: CoG, commissural ganglion; OG, oesophageal ganglion; STG, stomatogastric
1229 ganglion; Nerves: *dgn*, dorsal gastric nerve; *ion*, inferior oesophageal nerve; *lgn*, lateral
1230 gastric nerve; *lpgn* lateral posterior gastric nerve; *lvn*, lateral ventricular nerve; *mvn*,
1231 medial ventricular nerve; *on*, oesophageal nerve; *pdn*, pyloric dilator nerve; *son*,
1232 superior oesophageal nerve*; stn*, stomatogastric nerve; Neurons: AB, anterior burster;
1233 AM, anterior medial; DG, dorsal gastric; GM, gastric mill; IC, inferior cardiac; Int 1,

1234 interneuron 1; LG, lateral gastric; LP, lateral pyloric; LPG, lateral posterior gastric; MG,
1235 medial gastric; PD, pyloric dilator; PY, pyloric; VD, ventricular dilator.

1236

1237 **Figure 2. Gly^1-SIFamide modulates graded synaptic transmission between LG and**
1238 **LPG.**

1239 Intracellular two-electrode voltage clamp (TEVC) recordings were performed to examine
1240 synapses between LG and LPG. Symbols at the top indicate the synapse being tested
1241 in the left and right columns. ***A***, LPG was voltage clamped at -40 mV while LG was held
1242 at -60 mV and stepped from -55 mV to -20 mV in 5 mV increments (5 s duration, 11 s
1243 inter-step interval) in either TTX:Saline (***top***, black traces) or TTX:SIF (***bottom***, red
1244 traces). Grey arrows and grey trace indicate "bumps" in LPG voltage that occurred both
1245 during and between the LG voltage steps. Blue brackets indicate the time periods used
1246 for analysis. For each time point, the baseline current was subtracted from the peak
1247 current within that time window. ***Bi-Bii,*** LPG synaptic current in TTX:Saline (black) and
1248 TTX:SIF (red) as a function of LG voltage steps during the Early (***Bi***) and Late (***Bii***)
1249 component of the voltage step. Different shapes in Bi-Bii and Di-Dii represent individual
1250 experiments (n = 4). Insets indicate timepoints of measurements during an example
1251 voltage step. ***C,*** LPG was voltage clamped at -80 mV to eliminate spontaneous bursting
1252 activity of the other non-clamped LPG neuron between voltage steps and stepped to -55
1253 mV to -20 mV in 5 mV increments (5 s duration, 11 s inter-step interval) with LG held at
1254 -40 mV. 10 μM PTX was used to block glutamatergic transmission. Synaptic currents
1255 were measured in TTX:PTX:Saline (***top,*** black traces) and TTX:PTX:SIF (***bottom***, red
1256 traces). ***Di-Dii***, LG synaptic current as a function of LPG voltage steps during the Early

1257 (***Di***) and Late components of the LPG voltage step. #p < 0.05 TTX:Saline vs. TTX:SIF
1258 (Bi-ii) or TTX:PTX:Saline vs. TTX:PTX:SIF (Di-ii) at marked voltages (Two-way ANOVA,
1259 Holm-Sidak post hoc; see Table 1).

1260

1261 **Figure 3. Gly^1-SIFamide modulates graded synaptic transmission between IC and**
1262 **LPG.**
1263 Intracellular TEVC recordings were used to examine graded synapses between IC and
1264 LPG. Symbols at the top indicate the synapse being tested in the left and right columns.
1265 ***A***, LPG voltage clamped at -40 mV and IC stepped from -60 mV to -55 mV to -20 mV in
1266 5 mV increments in TTX:Saline (***top***, black traces) or TTX:SIF (***bottom***, red traces).
1267 Grey arrows indicate "bumps" in LPG voltage that occurred only during the IC voltage
1268 steps. ***Bi-Bii, Di-Dii,*** Same analysis as in figure 2A but for IC and LPG neurons (n = 5).
1269 ***C***, Example recordings of LPG held at -80 mV to eliminate spontaneous bursting activity
1270 of the other non-clamped LPG neuron between voltage steps and stepped to -55 mV to
1271 -20 mV with IC held at -40 mV. 10 μM PTX was used to block glutamatergic
1272 transmission. Synaptic currents were measured in TTX:PTX:Saline (***top*,** black traces)
1273 and TTX:PTX:SIF (***bottom***, red traces). #p < 0.05 TTX:Saline vs. TTX:SIF (Bi-ii) or
1274 TTX:PTX:Saline vs. TTX:PTX:SIF (Di-ii) at marked voltages (Two-way ANOVA, Holm-
1275 Sidak post hoc; see Table 2).

1276

1277

1278 **Figure 4. Gly^1-SIFamide modulates graded synaptic transmission from LPG to**
1279 **DG, but not DG to LPG.**
1280 Intracellular TEVC recordings were performed to examine synapses between DG and
1281 LPG. ***A***, Example recordings of LPG (voltage clamped at -40 mV) and DG held at -60
1282 mV and stepped from -55 mV to -20 mV in 5 mV increments in TTX:Saline (***top***, black
1283 traces) or TTX:SIF (***bottom***, red traces). LPG synaptic current as a function of DG
1284 voltage steps is plotted for Early (***Bi***) and Late (***Bii***) timepoints (n=4). ***C***, Example
1285 recordings of LPG voltage clamped at -80 mV and stepped to -55 mV to -20 mV with
1286 DG held at -40 mV. Synaptic currents were measured in TTX:PTX:Saline (***top,*** black
1287 traces) and TTX:PTX:SIF (***bottom***, red traces, transient in DG current trace truncated
1288 for presentation purposes). ***Di-Dii,*** DG synaptic current as a function of LPG voltage
1289 steps during Early (***Di***) and Late time points (n=5). $^{\#}p < 0.05$ TTX:Saline vs. TTX:SIF
1290 (Bi-ii) or TTX:PTX:Saline vs. TTX:PTX:SIF (Di-ii) at marked voltages (Two-way ANOVA,
1291 Holm-Sidak post hoc; see Table 3).

1292

1293

1294 **Figure 5. Graded synaptic transmission is sufficient for a coordinated gastric mill**
1295 **rhythm in Gly^1-SIFamide.**
1296 ***A***, Intracellular recordings of LPG, LG, IC, and DG during saline (***left***) and Gly^1-
1297 SIFamide application (***right***). In saline, only the pyloric rhythm was active, with LPG
1298 bursting in pyloric time with the PD neuron (*pdn*). In Gly^1-SIFamide, the gastric mill
1299 rhythm was activated (LG, DG, IC) and LPG generated both pyloric- and gastric mill-

1300 timed bursts. LPG pyloric-timed bursting in both saline and Gly^1-SIFamide was time-
1301 locked to the PD neuron *(pdn*). ***B,*** Tetrodotoxin (TTX) was applied to the preparation to
1302 block action potentials (***left***), then combined with Gly^1-SIFamide (***right***). LPG, LG, IC,
1303 and DG generated gastric mill-timed oscillations in the absence of action potentials
1304 during TTX + Gly^1-SIFamide application. The shaded region indicates one gastric mill
1305 cycle, using the LG neuron as a reference neuron. Note that LG and IC were co-active
1306 and out of phase with LPG and DG neurons, as in Gly^1-SIFamide application without
1307 TTX (***A***). Troughs in DG oscillations appeared to alternate with peaks in LPG
1308 oscillations (*dotted box*). LPG, LG, and IC also generated pyloric-timed oscillations
1309 (arrows and grey lines), suggesting that Gly^1-SIFamide also activated the pyloric rhythm
1310 without action potential-mediated transmission.

1311

1312 **Figure 6. LG entrained IC, DG, and LPG gastric mill neurons during Gly^1-SIFamide**
1313 **application.**
1314 All columns are from the same preparation, in which LG entrainment of test neurons IC
1315 (***Ai-iii***), DG (***Bi-iii***), and LPG (***Ci-iii***) was examined. In Gly^1-SIFamide (5 μM) prior to any
1316 manipulations, LG burst frequency was approximately 0.03 Hz and IC, DG, and LPG
1317 were bursting (***Ai-Ci***, No Entrainment). Dotted line indicates one LG cycle. ***Aii-Cii,*** To
1318 determine the ability of LG to entrain the other neurons, LG was rhythmically
1319 depolarized (*upward arrowheads*, 5 s duration; LG recordings are omitted for clarity) at
1320 different entrainment frequencies, and IC (***Aii***), DG (***Bii***), and LPG (***Cii***) activity
1321 recorded. IC is active in both pyloric and gastric mill time during the Gly^1-SIFamide
1322 rhythm, but only its gastric mill bursts were analyzed. IC gastric mill bursts (boxes) were

identified as in previous studies (12, 21)(see Methods). ***Aiii-Ciii,*** Instantaneous gastric mill burst frequency of IC (***Aiii***), DG (***Biii***), and LPG (***Ciii***) was plotted as a function of LG entrainment frequency. Each colored data point is the instantaneous burst frequency for one cycle (1/duration between two consecutive bursts), and each color represents data from a single preparation. Solid diagonal line indicates perfect entrainment (1:1), where instantaneous burst frequency was equal to entrainment frequency. Dashed diagonal lines indicate other modes of entrainment at which test neuron burst frequency would be a multiple, or a fraction, of entrainment frequency. Data points that fall between diagonal lines indicate a lack of LG entrainment of that neuron burst. Numbers of instantaneous burst frequencies plotted at each frequency are presented in Table 4. ***D,*** The cumulative distribution frequency (c.d.f.) of significands are overlaid for LPG (*light grey*), DG (*dark grey*), and IC (*black*) responses to an LG entrainment frequency of 0.06 Hz. Significands are the value to the right of the decimal after dividing each instantaneous burst frequency of IC, LPG, or DG by the LG entrainment frequency. The red diagonal line represents a c.d.f. where significands are randomly distributed between 0 and 1, indicating no entrainment. The blue dotted line represents a c.d.f. with a large portion of the distribution close to 0 and/or 1, indicating entrainment. Shaded regions indicate the area between the c.d.f. for each neuron and the diagonal line. Insets of c.d.f. graphs enable visualization of area for each neuron separately. ***E,*** Area between the significand c.d.f. curve and the diagonal line for IC (*black*), DG (*dark grey*), and LPG (*light grey*) as a function of LG entrainment frequency. The arrow and vertical dotted line indicate the c.d.f. area for the 0.06 Hz c.d.f. histograms plotted in (***D***) (other c.d.f.s are presented in Supplemental Fig. S1). The horizontal dashed line at 0.25

1346 indicates one example of perfect entrainment, calculated as the area between the
1347 dotted blue line and the red diagonal line in (***D***). The c.d.f. for each neuron at each
1348 entrainment frequency was compared to a uniform distribution indicating zero integer
1349 coupling (i.e., diagonal line) to test for statistical significance using the Kolmogorov-
1350 Smirnoff test with a corrected alpha level of 0.007 (see Methods). Area values different
1351 from the uniform distribution at each entrainment frequency are indicated above the
1352 graph for each neuron pair. *$p < 0.007$, $^{ns}p > 0.007$ (see Table 5). Dash indicates data
1353 was not obtained at that entrainment frequency.

1354

1355 **Figure 7. IC and DG entrained the other gastric mill neurons during Gly^{1}-SIFamide**
1356 **application at some entrainment frequencies.**
1357 ***Ai,*** Overlaid cumulative distribution frequency histograms (c.d.f.s) for IC entrainment
1358 frequency of 0.06 Hz for LG (*light grey*), DG (*dark grey*), and LPG (*black*). ***Bi***, Overlaid
1359 c.d.f.s for DG entrainment frequency of 0.06 Hz for LPG (*light grey*), IC (*dark grey*), and
1360 LG (*black*). Area between the significand c.d.f. curve and the red diagonal line for LG
1361 (*light grey*), DG (*dark grey*), and LPG (*black*) as a function of IC entrainment frequency
1362 (***Aii***) or LPG (*light grey*), IC (*dark grey*), and LG (*black*) as a function of DG entrainment
1363 frequency (***Bii***). The arrow and vertical dotted lines indicate the c.d.f. area calculated for
1364 the 0.06 Hz c.d.f. histograms plotted in (***Ai, Bi***) (other c.d.f.s are presented in
1365 Supplemental Figs. S3, S5). The c.d.f. for each neuron at each entrainment frequency
1366 was compared to a uniform distribution indicating zero integer coupling (i.e., diagonal
1367 line) to test for statistical significance using the Kolmogorov-Smirnoff test with a
1368 corrected alpha level of 0.007 (See Methods). Area values different from the uniform

1369 distribution at each entrainment frequency are indicated above the graph for each
1370 neuron pair. *p < 0.007, ^{ns}p > 0.007 (see Table 5). Dash indicates data was not
1371 obtained at that entrainment frequency.

1372

1373 **Figure 8. LPG entrainment of LG, IC, and DG gastric mill neurons during Gly^{1}-**
1374 **SIFamide (SIF) and Gly^{1}-SIFamide plus picrotoxin (SIF:PTX) application.**
1375 ***Ai,*** Overlaid cumulative distribution frequency histograms (c.d.f.s) for LPG entrainment
1376 frequency of 0.06 Hz for IC (*light grey*), LG (*dark grey*), and DG (*black*) during Gly^{1}-
1377 SIFamide (SIF) application. ***Bi***, Overlaid c.d.f.s for LPG entrainment frequency of 0.06
1378 Hz for IC (*light grey*), LG (*dark grey*), and DG (*black*) during Gly^{1}-SIFamide plus
1379 picrotoxin (SIF:PTX) application. Area between the significand c.d.f. curve and the red
1380 diagonal line for IC (*light grey*), LG (*dark grey*), and DG (*black*) as a function of LPG
1381 entrainment frequency during SIF (***Aii***) or SIF:PTX (***Bii***). The arrow and vertical dotted
1382 lines indicate the c.d.f. area calculated for the 0.06 Hz c.d.f. histograms plotted in (***Ai,***
1383 ***Bi***) (other c.d.f.s are presented in Supplemental Figs. S7, S9). The c.d.f. for each
1384 neuron at each entrainment frequency was compared to a uniform distribution indicating
1385 zero integer coupling (i.e., diagonal line) to test for statistical significance using the
1386 Kolmogorov-Smirnoff test with a corrected alpha level of 0.007 (See Methods). Area
1387 values different from the uniform distribution at each entrainment frequency are
1388 indicated above the graph for each neuron pair. *p < 0.007, ^{ns}p > 0.007 (see Table 6).
1389 Dash indicates data was not obtained at that entrainment frequency.

1390

1391 **Figure 9. Gly^1-SIFamide modulates multiple synapses.**

1392 Updated partial circuit diagram from figure 1. ***A, Left,*** In saline conditions (Saline), the
1393 pyloric neuron LPG is electrically coupled to the AB/PD pyloric pacemaker ensemble,
1394 and receives a weak chemical inhibitory synapse from IC. The gastric mill rhythm is off.
1395 ***Right***, During Gly^1-SIFamide application, LPG intrinsic properties are modulated to
1396 enable LPG switching into dual pyloric plus gastric mill activity (red/blue LPG circle).
1397 Gly^1-SIFamide modulation also enhances bidirectional chemical inhibitory synapses
1398 between LPG and the IC, LG, and DG gastric mill neurons. ***B***, Potential additional
1399 inhibitory chemical synapses that are functional during Gly^1-SIFamide application
1400 among the LG, IC, and DG neurons, based on results of entrainment experiments.
1401 Additionally, entrainment data suggests that the established electrical coupling between
1402 IC and LG may be rectifying (*diode*), such that positive current flows better from LG to
1403 IC. Resistor and diode, electrical coupling; ball and stick, chemical inhibition, thickness
1404 indicates relative synapse strength; red circles, pyloric neurons; blue circles, gastric mill
1405 neurons; red/blue circles; gastropyloric neurons.

1406

1407 Table 1. Effects of voltage and Gly[1]-SIFamide on synaptic currents between LG and LPG, at
1408 early and late time windows in the voltage step.

		Voltage Step: Early			Voltage Step: Late		
		p values (t)			p values (t)		
		Voltage-Dependence			Voltage-Dependence		
Neurons	Voltage (mV)	TTX	TTX:SIF	TTX vs TTX:SIF	TTX	TTX:SIF	TTX vs TTX:SIF
LG to LPG (n = 4)	-55 vs -20	0.999 (1.227)	0.003 (4.204)		1.000 (0.998)	<0.001 (5.283)	
	-55			0.951 (0.063)			0.382 (0.895)
	-50			0.574 (0.582)			0.624 (0.499)
	-45			0.862 (0.179)			0.168 (1.430)
	-40			0.192 (1.410)			0.102 (1.715)
	-35			0.008 (3.414)			<0.001 (4.715)
	-30			0.055 (2.196)			<0.001 (4.805)
	-25			0.03 (2.573)			<0.001 (4.896)
	-20			0.046 (2.315)			<0.001 (5.074)
LPG to LG[a] (n = 4)	-55 vs -20	ns		ns	1.000 (0.162)	<0.001 (6.360)	
	-55						0.254 (1.346)
	-50						0.117 (2.031)
	-45						0.101 (2.168)
	-40						0.072 (2.488)
	-35						0.044 (2.986)
	-30						0.042 (3.021)
	-25						0.023 (3.709)
	-20						0.029 (3.450)

1409 Two-way repeated measures (RM) ANOVA analysis with condition (TTX:Saline vs. TTX:SIF),
1410 and voltage as the two main effects, followed by post-hoc Holm-Sidak pairwise comparisons.
1411 [a]PTX included in TTX:Saline and TTX:SIF solutions to block glutamatergic transmission when
1412 testing the LPG to LG synapse. [ns]RM ANOVA p> 0.05, no post-hoc tests performed.

1413

1414 Table 2. Effects of voltage and Gly[1]-SIFamide on synaptic currents between IC and LPG, at
1415 early and late time windows in the voltage step.

		Voltage Step: Early			Voltage Step: Late		
		p values (t)			p values (t)		
		Voltage-Dependence			Voltage-Dependence		
Neurons	Voltage (mV)	TTX	TTX:SIF	TTX vs TTX:SIF	TTX	TTX:SIF	TTX vs TTX:SIF
IC to LPG (n = 5)	-55 vs -20	0.059 (3.267)	<0.001 (6.121)		0.070 (3.155)	<0.001 (7.086)	
	-55			0.071 (2.445)			0.498 (0.705)
	-50			0.640 (0.483)			0.617 (0.517)
	-45			0.407 (0.869)			0.317 (0.940)
	-40			0.132 (1.652)			0.085 (1.930)
	-35			0.032 (2.516)			0.027 (2.636)
	-30			0.020 (2.810)			0.006 (3.522)
	-25			0.008 (3.352)			0.004 (3.835)
	-20			0.007 (3.495)			0.003 (3.959)
LPG to IC[a] (n = 5)	-55 vs -20	0.335 (2.528)	<0.001 (5.177)		0.972 (1.565)	<0.001 (8.036)	
	-55			0.057 (2.529)			0.032 (2.903)
	-50			0.028 (3.185)			0.014 (3.601)
	-45			0.019 (3.551)			0.004 (4.840)
	-40			0.017 (3.658)			0.007 (4.372)
	-35			0.014 (3.879)			0.003 (5.169)
	-30			0.011 (4.128)			0.002 (5.560)
	-25			0.011 (4.162)			0.003 (5.431)
	-20			0.006 (4.904)			<0.001 (6.926)

1416 Two-way repeated measures (RM) ANOVA analysis with condition (TTX:Saline vs. TTX:SIF),
1417 and voltage as the two main effects, followed by post-hoc Holm-Sidak pairwise comparisons.
1418 [a]PTX included in TTX:Saline and TTX:SIF solutions to block glutamatergic transmission when
1419 testing the LPG to IC synapse.

1420 Table 3. Effects of voltage and Gly[1]-SIFamide on synaptic currents between DG and LPG, at
1421 early and late time windows in the voltage step.

		Voltage Step: Early			Voltage Step: Late		
		p values (t)			p values (t)		
		Voltage-Dependence			Voltage-Dependence		
Neurons	Voltage (mV)	TTX	TTX:SIF	TTX vs TTX:SIF	TTX	TTX:SIF	TTX vs TTX:SIF
DG to LPG (n = 4)	-55 vs -20	0.415 (2.459)	<0.001 (4.996)		0.190 (2.848)	<0.001 (6.262)	
	-55			0.294 (1.187)			0.207 (1.521)
	-50			0.274 (1.244)			0.205 (1.528)
	-45			0.139 (1.793)			0.137 (1.883)
	-40			0.101 (2.054)			0.136 (1.885)
	-35			0.064 (2.441)			0.064 (2.593)
	-30			0.134 (1.826)			0.104 (2.126)
	-25			0.137 (1.804)			0.099 (2.178)
	-20			0.103 (2.036)			0.072 (2.476)
LPG to DG[a] (n = 5)	-55 vs -20	1.000 (0.156)	<0.001 (6.058)		1.000 (0.128)	<0.001 (7.501)	
	-55			0.177 (1.605)			0.131 (1.807)
	-50			0.073 (2.342)			0.065 (2.363)
	-45			0.100 (2.072)			0.062 (2.396)
	-40			0.078 (2.283)			0.043 (2.700)
	-35			0.043 (2.816)			0.034 (2.902)
	-30			0.057 (2.556)			0.024 (3.199)
	-25			0.033 (3.066)			0.010 (4.042)
	-20			0.035 (3.003)			0.007 (4.413)

1422 Two-way repeated measures (RM) ANOVA analysis with condition (TTX:Saline vs. TTX:SIF),
1423 and voltage as the two main effects, followed by post-hoc Holm-Sidak pairwise comparisons.
1424 [a]PTX included in TTX:Saline and TTX:SIF solutions to block glutamatergic transmission when
1425 testing the LPG to DG synapse.

1426 Table 4. Number of test neuron cycles per preparation from each LG, IC, and DG entrainment
1427 frequency in Gly[1]-SIFamide.

LG Entrainment Neuron				IC Entrainment Neuron				DG Entrainment Neuron			
Test Neuron	Entrain Freq (Hz)	# Cycles / Prep	*n*	Test Neuron	Entrain Freq (Hz)	# Cycles / Prep	*n*	Test Neuron	Entrain Freq (Hz)	# Cycles / Prep	*n*
	0.03	9-10	3		0.03	--	-		0.03	9-18	3
	0.04	--	-		0.04	4-22	2		0.04	12-19	4
	0.05	--	-		0.05	8-13	4		0.05	7-18	6
IC	0.06	8-14	7	LG	0.06	6-11	5	LG	0.06	5-11	8
	0.075	8-10	6		0.075	2-9	6		0.075	3-10	8
	0.09	10-11	7		0.09	5-8	4		0.09	2-9	8
	0.12	4-14	7		0.12	4-6	4		0.12	1-9	7
	0.03	--	-		0.03	4-18	3		0.03	12-14	2
	0.04	--	-		0.04	6-11	3		0.04	9-18	4
	0.05	8-9	2		0.05	9-11	3		0.05	9-17	5
DG	0.06	3-9	7	DG	0.06	2-10	8	IC	0.06	2-10	8
	0.075	2-9	6		0.075	1-10	8		0.075	6-10	7
	0.09	1-9	6		0.09	1-10	7		0.09	3-9	7
	0.12	1-9	7		0.12	1-10	7		0.12	4-7	6
	0.03	23-29	3		0.03	6-28	4		0.03	15-29	3
	0.04	--	-		0.04	15-19	3		0.04	10-21	5
	0.05	14-19	2		0.05	6-12	4		0.05	6-18	6
LPG	0.06	9-20	8	LPG	0.06	7-10	9	LPG	0.06	9-16	11
	0.075	8-10	7		0.075	3-10	9		0.075	7-14	10
	0.09	8-10	8		0.09	3-9	8		0.09	5-12	11
	0.12	5-9	8		0.12	1-11	8		0.12	4-10	11

1428

1429

1430

1431

1432

1433

1434 Table 5. Statistical analysis of the ability of LG, IC, and DG to entrain the other gastric mill
1435 neurons during Gly[1]-SIFamide application.
1436

	p value (D)								
	Entrainment/Test Neuron								
Entrainment Frequency	LG/IC	LG/DG	LG/LPG	IC/LG	IC/DG	IC/LPG	DG/LG	DG/IC	DG/LPG
0.03	<0.001 (0.902)	---	<0.001 (0.284)	---	0.271 (0.137)	<0.001 0.324)	<0.001 (0.353)	0.003 (0.245)	0.025 (0.206)
0.04	---	---	---	0.001 (0.265)	<0.001 (0.382)	<0.001 (0.275)	0.360 (0.127)	0.074 (0.176)	<0.001 (0.324)
0.05	---	<0.001 (0.725)	0.001 (0.265)	0.051 (0.186)	<0.001 (0.520)	<0.001 (0.363)	<0.001 (0.353)	<0.001 (0.373)	<0.001 (0.441)
0.06	<0.001 (0.509)	<0.001 (0.324)	0.034 (0.196)	0.0057 (0.235)	<0.001 (0.275)	<0.001 (0.451)	<0.001 (0.600)	<0.001 (0.647)	0.002 (0.255)
0.075	<0.001 (0.520)	<0.001 (0.559)	<0.001 (0.520)	0.051 (0.186)	<0.001 (0.461)	<0.001 (0.608)	<0.001 (0.627)	<0.001 (0.529)	0.014 (0.216)
0.09	<0.001 (0.431)	<0.001 (0.676)	<0.001 (0.461)	0.034 (0.196)	<0.001 (0.539)	<0.001 (0.422)	<0.001 (0.412)	<0.001 (0.392)	0.001 (0.265)
0.12	0.074 (0.176)	<0.001 (0.392)	<0.001 (0.284)	<0.001 (0.353)	<0.001 (0.520)	0.003 (0.245)	<0.001 (0.471)	<0.001 (0.363)	0.051 (0.186)

1437 Two-sample Kolmogorov-Smirnov test was used to compare each c.d.f. to a uniform
1438 distribution, alpha level was 0.007 to correct for multiple comparisons

1439

1440

1441

1442

1443

1444

1445

1446

1447 Table 6. Number of test neuron cycles per preparation from each LPG entrainment frequency in
1448 Gly[1]-SIFamide (SIF) and Gly[1]-SIFamide plus PTX (SIF:PTX), and statistical analysis of
1449 entrainment.
1450

LPG Entrainment Neuron (SIF)					LPG Entrainment Neuron (SIF:PTX)				
Test Neuron	Entrain Freq (Hz)	# Cycles/ Prep	*n*	p value (D)	Test Neuron	Entrain Freq (Hz)	# Cycles/ Prep	*n*	p value (D)
LG	0.03	10-20	2	<0.001 (0.314)	LG	0.03	11-21	4	<0.001 (0.363)
	0.04	10-17	4	0.271 (0.137)		0.04	8-27	4	<0.001 (0.353)
	0.05	9-18	5	0.689 (0.098)		0.05	9	3	<0.001 (0.549)
	0.06	5-16	6	0.009 (0.225)		0.06	7-12	7	<0.001 (0.441)
	0.075	5-12	6	<0.001 (0.304)		0.075	4-9	7	<0.001 (0.333)
	0.09	4-9	5	<0.001 (0.333)		0.09	1-9	7	<0.001 (0.520)
	0.12	3-10	5	0.015 (0.216)		0.12	1-9	7	<0.001 (0.275)
IC	0.03	--	-	--	IC	0.03	7-14	4	<0.001 (0.431)
	0.04	10-12	4	0.034 (0.196)		0.04	1-11	5	<0.001 (0.618)
	0.05	9-17	5	0.020 (0.147)		0.05	6-10	4	<0.001 (0.814)
	0.06	5-16	5	0.034 (0.196)		0.06	5-16	8	<0.001 (0.412)
	0.075	4-12	5	<0.001 (0.373)		0.075	1-10	8	<0.001 (0.373)
	0.09	3-9	5	<0.001 (0.314)		0.09	3-12	8	<0.001 (0.402)
	0.12	3-9	5	0.051 (0.186)		0.12	2-8	8	<0.001 (0.353)
DG	0.03	--	-	--	DG	0.03	11-16	4	0.356 (0.127)
	0.04	6-10	4	<0.001 (0.637)		0.04	9-12	5	<0.001 (0.461)
	0.05	7-12	5	<0.001 (0.559)		0.05	9-10	4	<0.001 (0.569)
	0.06	1-10	7	<0.001 (0.451)		0.06	5-10	8	<0.001 (0.539)
	0.075	2-10	7	<0.001 (0.696)		0.075	3-9	8	<0.001 (0.5)
	0.09	2-10	7	<0.001 (0.471)		0.09	3-10	8	<0.001 (0.490)
	0.12	1-10	7	<0.001 (0.480)		0.12	2-8	7	<0.001 (0.392)

1451 Two-sample Kolmogorov-Smirnov test to compare each c.d.f. to a uniform distribution, alpha
1452 level was 0.007 to correct for multiple comparisons

1453

1454 **Supplemental Figure S1. LG entrainment of IC (*left*), DG (*middle*), and LPG (*right*)**
1455 **during Gly^1-SIFamide.**
1456 C.d.f. graphs for IC (n = 3-7), DG (n = 2-7), and LPG (n = 2-8) neurons during LG
1457 entrainment, with each row indicating the entrainment frequency. Missing graphs
1458 indicate excluded data that was n = 1, or data that was not collected for that frequency.
1459

1460 **Supplemental Figure S2. IC entrainment of LG, DG, and LPG gastric mill neurons**
1461 **during Gly^1-SIFamide application.**
1462 ***Ai-Ci, Aii-Cii,*** All columns are from the same preparation, in which IC entrainment of
1463 test neurons LG (*lgn,* ***Ai-iii***), DG (*dgn,* ***Bi-iii***), and LPG (*lpgn,* ***Ci-iii***) was examined. In
1464 Gly^1-SIFamide (5 μM) prior to any manipulations, IC burst frequency was approximately
1465 0.05 Hz and IC, DG, and LPG were bursting (***Ai-Ci***, No Entrainment). ***Aii-Cii***, To
1466 determine the ability of IC to entrain the other neurons, IC was rhythmically depolarized
1467 (*upward arrowheads*, 5 s duration; IC recordings are omitted for clarity) at different
1468 entrainment frequencies, and LG (*lgn,* ***Aii***), DG (*dgn,* ***Bii***), and LPG (*lpgn,* ***Cii***) activity
1469 recorded. ***Aiii-Ciii,*** Instantaneous burst frequency of LG (***Aiii***), DG (***Biii***), and LPG (***Ciii***)
1470 was plotted as a function of IC entrainment frequency. Each colored data point is one
1471 instantaneous burst frequency from one preparation. Solid diagonal line indicates
1472 perfect entrainment (1:1), where instantaneous burst frequency was equal to
1473 entrainment frequency. Dashed diagonal lines indicate other modes of entrainment at
1474 which test neuron burst frequency would be a multiple, or a fraction, of entrainment
1475 frequency. Data points that fall between diagonal lines indicate a lack of IC entrainment
1476 of that neuron burst.

1477

1478 **Supplemental Figure S3. IC entrainment of LG (*left*), DG (*middle*), and LPG (*right*)**

1479 **during Gly^1-SIFamide.**

1480 C.d.f. graphs for LG (n = 2-6), DG (n = 3-8), and LPG (n = 2-9) neurons during IC

1481 entrainment, with each row indicating the entrainment frequency. Missing graphs

1482 indicate excluded data that was n = 1, or data that was not collected for that frequency.

1483

1484 **Supplemental Figure S4. DG entrainment of LG, IC, and LPG gastric mill neurons**

1485 **during Gly^1-SIFamide application.**

1486 ***Ai-Ci, Aii-Cii***, All columns are from the same preparation, in which DG entrainment of

1487 test neurons LG (*lgn,* ***Ai-iii***), IC (*mvn,* ***Bi-iii***), and LPG (*lpgn,* ***Ci-iii***) was examined. In

1488 Gly^1-SIFamide (5 μM) prior to any manipulations, DG burst frequency was

1489 approximately 0.04 Hz and LG, IC, and LPG were bursting (***Ai-Ci***, No Entrainment). ***Aii-***

1490 ***Cii,*** To determine the ability of DG to entrain the other neurons, DG was rhythmically

1491 depolarized (*upward arrowheads*, 5 s duration; DG recordings are omitted for clarity) at

1492 different entrainment frequencies, and LG (*lgn,* ***Aii***), IC (*mvn,* ***Bii***), and LPG (*lpgn,* ***Cii***)

1493 activity recorded. ***Aiii-Ciii***. Instantaneous burst frequency of LG (***Aiii***), IC (***Biii***), and

1494 LPG (***Ciii***) was plotted as a function of DG entrainment frequency. Each colored data

1495 point is one instantaneous burst frequency from one preparation. Solid diagonal line

1496 indicates perfect entrainment (1:1), where instantaneous burst frequency was equal to

1497 entrainment frequency. Dashed diagonal lines indicate other modes of entrainment at

1498 which test neuron burst frequency would be a multiple, or a fraction, of entrainment

1499 frequency. Data points that fall between diagonal lines indicate a lack of DG

1500 entrainment of that neuron burst.

1501

1502 **Supplemental Figure S5**. **DG entrainment of LG (*left*), IC (*middle*), and LPG (*right*)**

1503 **during Gly^1-SIFamide.**

1504 C.d.f. graphs for LG (n = 3-8), IC (n = 2-8), and LPG (n = 3-11) neurons during DG

1505 entrainment, with each row indicating the entrainment frequency.

1506

1507 **Supplemental Figure S6. LPG entrainment of LG, IC, and DG gastric mill neurons**

1508 **during Gly^1-SIFamide application.**

1509 ***Ai-Ci, Aii-Cii***, All columns are from the same preparation, in which LPG entrainment of

1510 test neurons LG (*lgn,* ***Ai-iii***), IC (*mvn,* ***Bi-iii***), and DG (*dgn,* ***Ci-iii***) was examined. In

1511 Gly^1-SIFamide (5 μM) prior to any manipulations, LPG burst frequency was

1512 approximately 0.05 Hz and LG, IC, and DG were bursting (***Ai-Ci***, No Entrainment). ***Aii-***

1513 ***Cii,*** To determine the ability of LPG to entrain the other neurons, LPG was rhythmically

1514 depolarized (*upward arrowheads*, 5 s duration; LPG recordings are omitted for clarity) at

1515 different entrainment frequencies, and LG (*lgn,* ***Aii***), IC (*mvn,* ***Bii***), and DG (*dgn,* ***Cii***)

1516 activity recorded. ***Aiii-Ciii***. Instantaneous burst frequency of LG (***Aiii***), IC (***Biii***), and DG

1517 (***Ciii***) was plotted as a function of LPG entrainment frequency. Each colored data point

1518 is one instantaneous burst frequency from one preparation. Solid diagonal line indicates

1519 perfect entrainment (1:1), where instantaneous burst frequency was equal to

1520 entrainment frequency. Dashed diagonal lines indicate other modes of entrainment at

1521 which test neuron burst frequency would be a multiple, or a fraction, of entrainment

1522 frequency. Data points that fall between diagonal lines indicate a lack of LPG

1523 entrainment of that neuron burst.

1524

1525 **Supplemental Figure S7**. **LPG entrainment of LG (*left*), IC (*middle*), and DG (*right*)**

1526 **during Gly^1-SIFamide.**

1527 C.d.f. graphs for LG (n = 2-6), IC (n = 4-5), and DG (n = 4-7) neurons during LPG

1528 entrainment, with each row indicating the entrainment frequency. Missing graphs

1529 indicate excluded data that was n = 1, or data that was not collected for that frequency.

1530

1531 **Supplemental Figure S8. LPG entrainment of LG, IC, and DG gastric mill neurons**

1532 **during Gly^1-SIFamide plus picrotoxin (SIF:PTX) application.**

1533 ***Ai-Ci, Aii-Cii***, All columns are from the same preparation, in which LPG entrainment of

1534 test neurons LG (*lgn,* ***Ai-iii***), IC (*mvn,* ***Bi-iii***), and DG (*dgn,* ***Ci-iii***) was examined during

1535 Gly^1-SIFamide (5 μM) plus picrotoxin (10 μM) (SIF:PTX). Prior to any manipulations,

1536 LPG burst frequency was approximately 0.06 Hz and LG, IC, and DG were bursting (***Ai-***

1537 ***Ci***, No Entrainment). ***Aii-Cii,*** To determine the ability of LPG to entrain the other

1538 neurons, LPG was rhythmically depolarized (*upward arrowheads*, 5 s duration; LPG

1539 recordings are omitted for clarity) at different entrainment frequencies, and LG (*lgn,* ***Aii***),

1540 IC (*mvn,* ***Bii***), and DG (*dgn,* ***Cii***) activity recorded. ***Aiii-Ciii***. Instantaneous burst

1541 frequency of LG (***Aiii***), IC (***Biii***), and DG (***Ciii***) was plotted as a function of LPG

1542 entrainment frequency. Each colored data point is one instantaneous burst frequency

1543 from one preparation. Solid diagonal line indicates perfect entrainment (1:1), where

1544 instantaneous burst frequency was equal to entrainment frequency. Dashed diagonal

1545 lines indicate other modes of entrainment at which test neuron burst frequency would be

1546 a multiple, or a fraction, of entrainment frequency. Data points that fall between diagonal

1547 lines indicate a lack of LPG entrainment of that neuron burst.

1548

1549 **Supplemental Figure S9. LPG entrainment of LG (*left*), IC (*middle*), and DG (*right*)**

1550 **during Gly^{1}-SIFamide plus picrotoxin (SIF:PTX).**

1551 C.d.f. graphs for LG (n = 4-7), IC (n = 4-8), and DG (n = 4-8) neurons during LPG

1552 entrainment, with each row indicating the entrainment frequency.

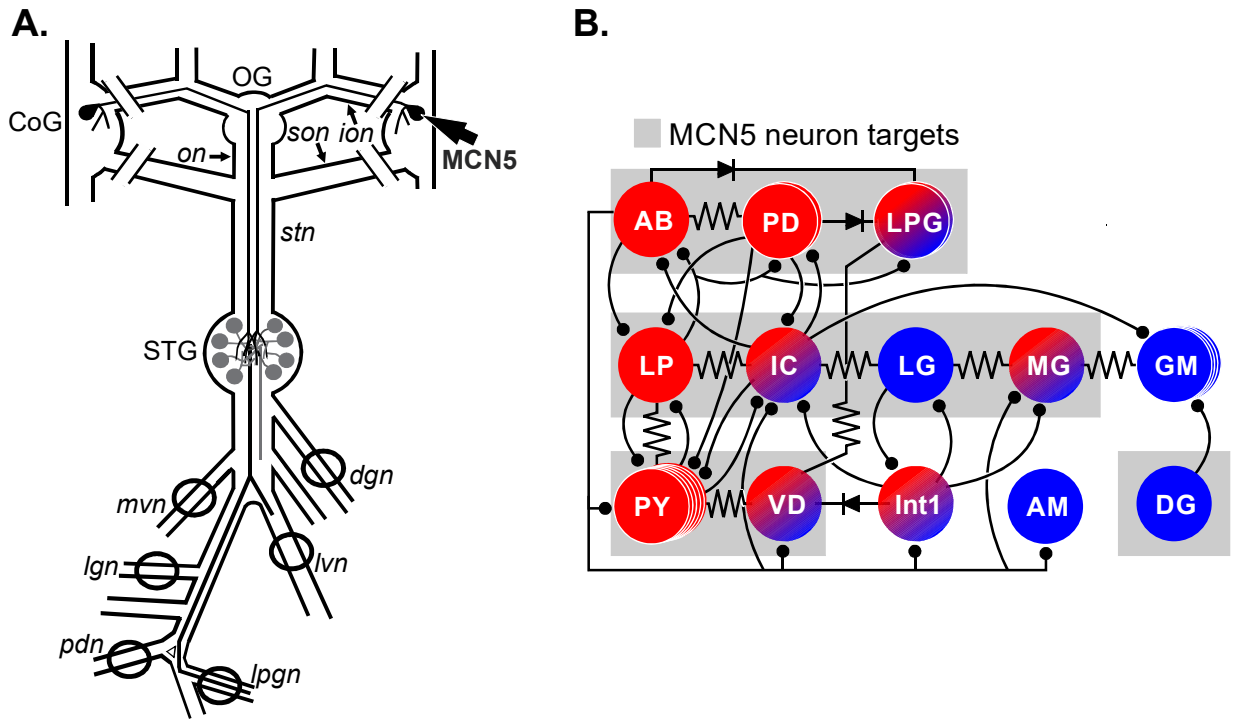

Figure 1
Fahoum and Blitz

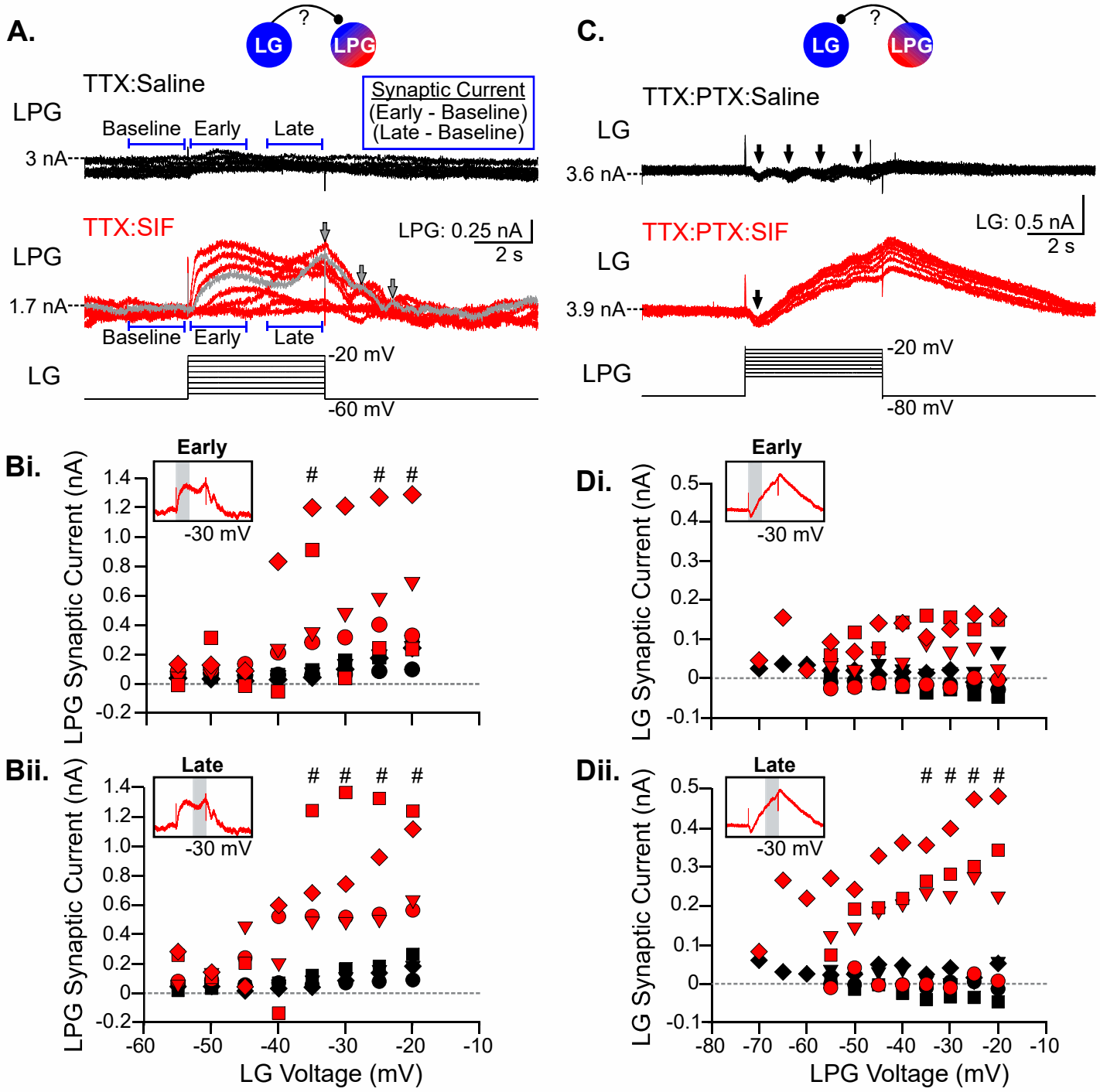

Figure 2
Fahoum and Blitz

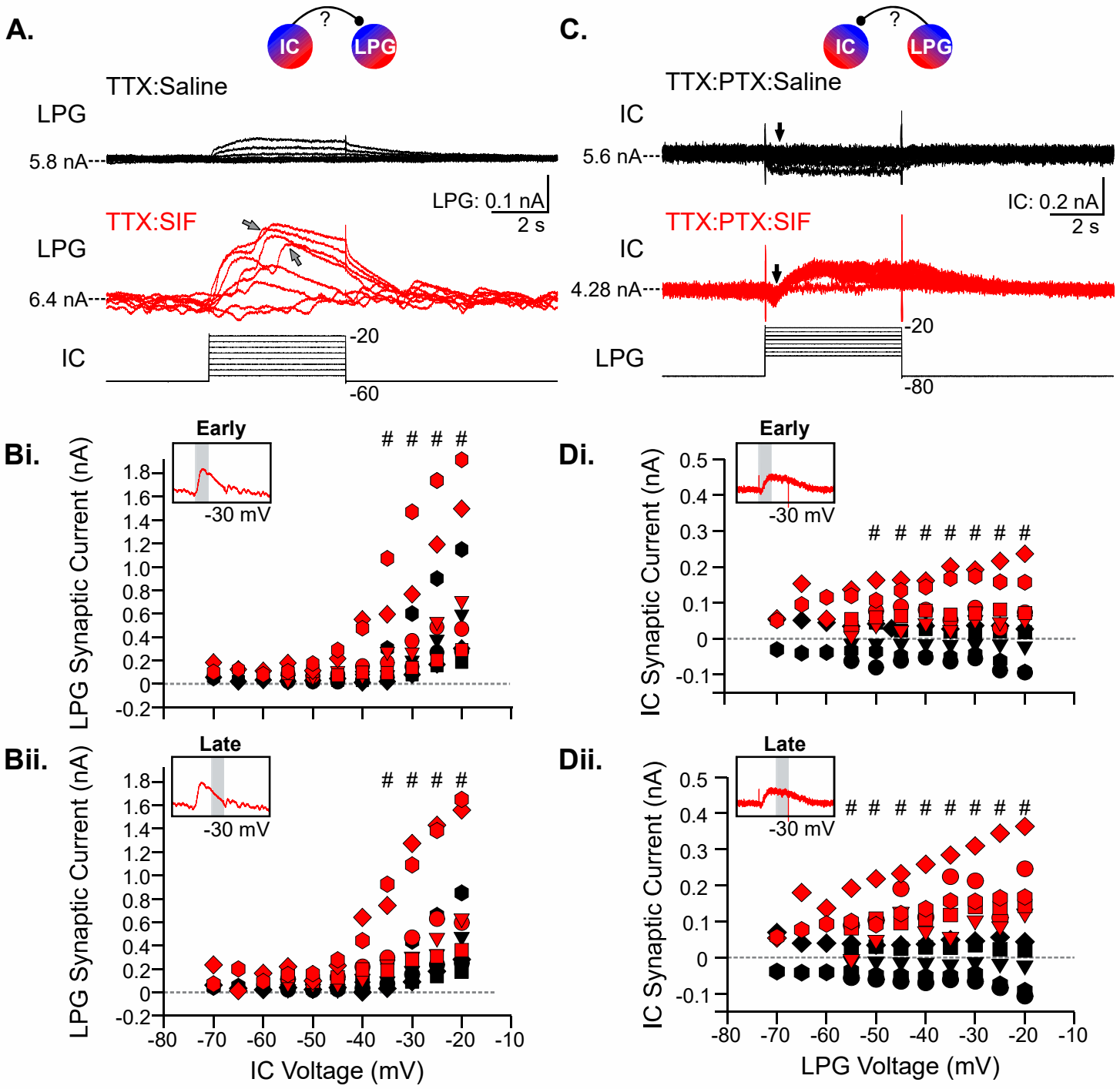

Figure 3
Fahoum and Blitz

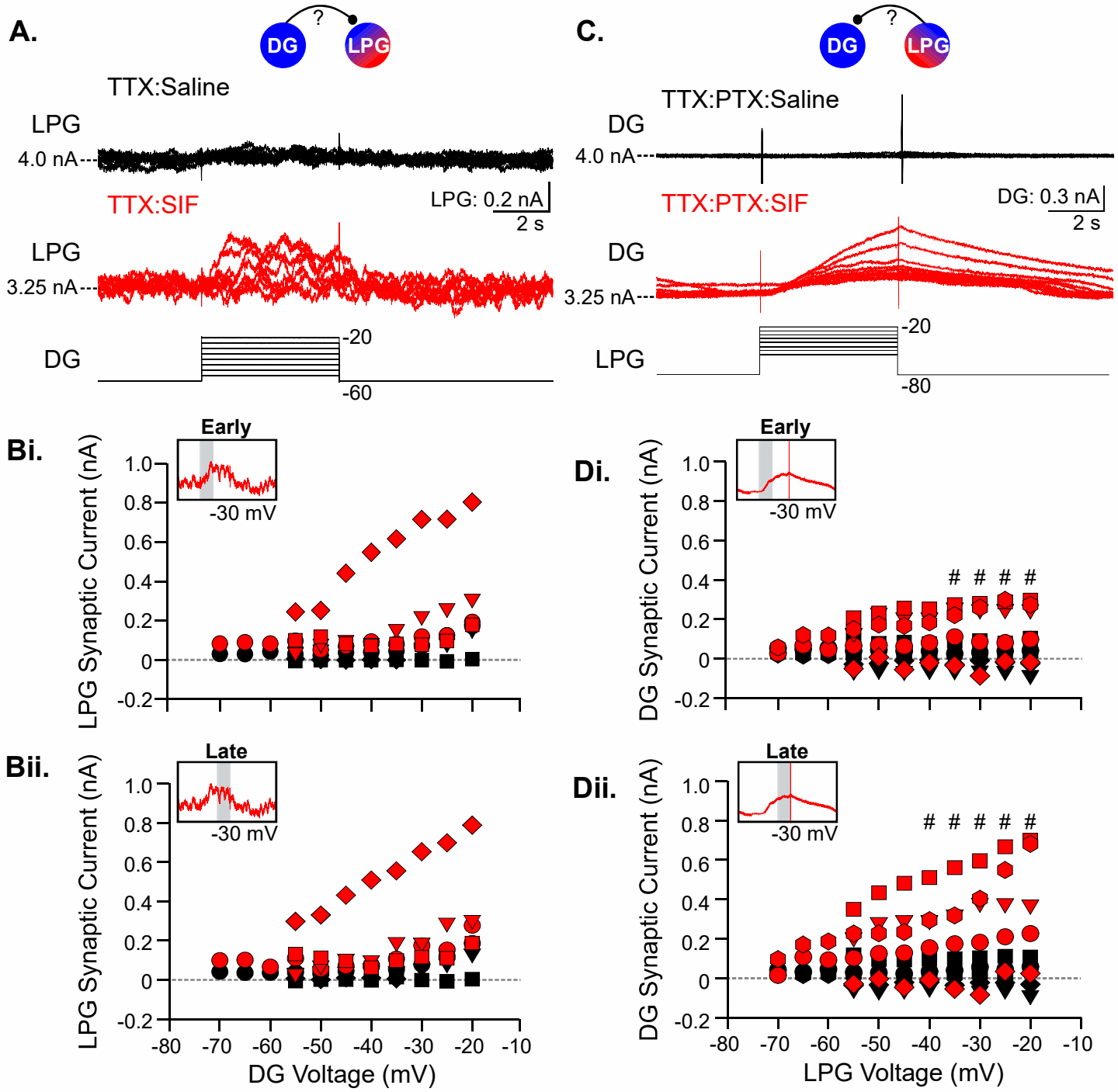

Figure 4
Fahoum and Blitz

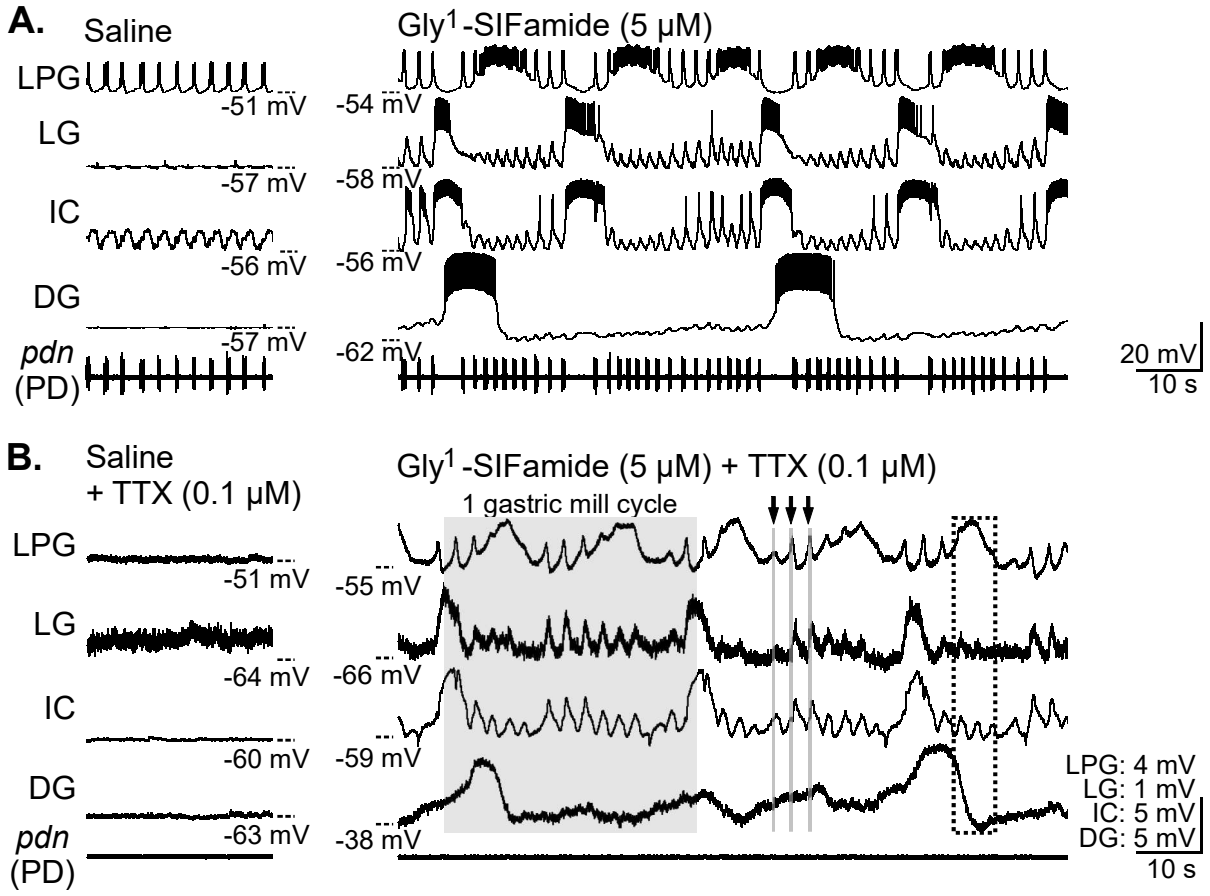

Figure 5
Fahoum and Blitz

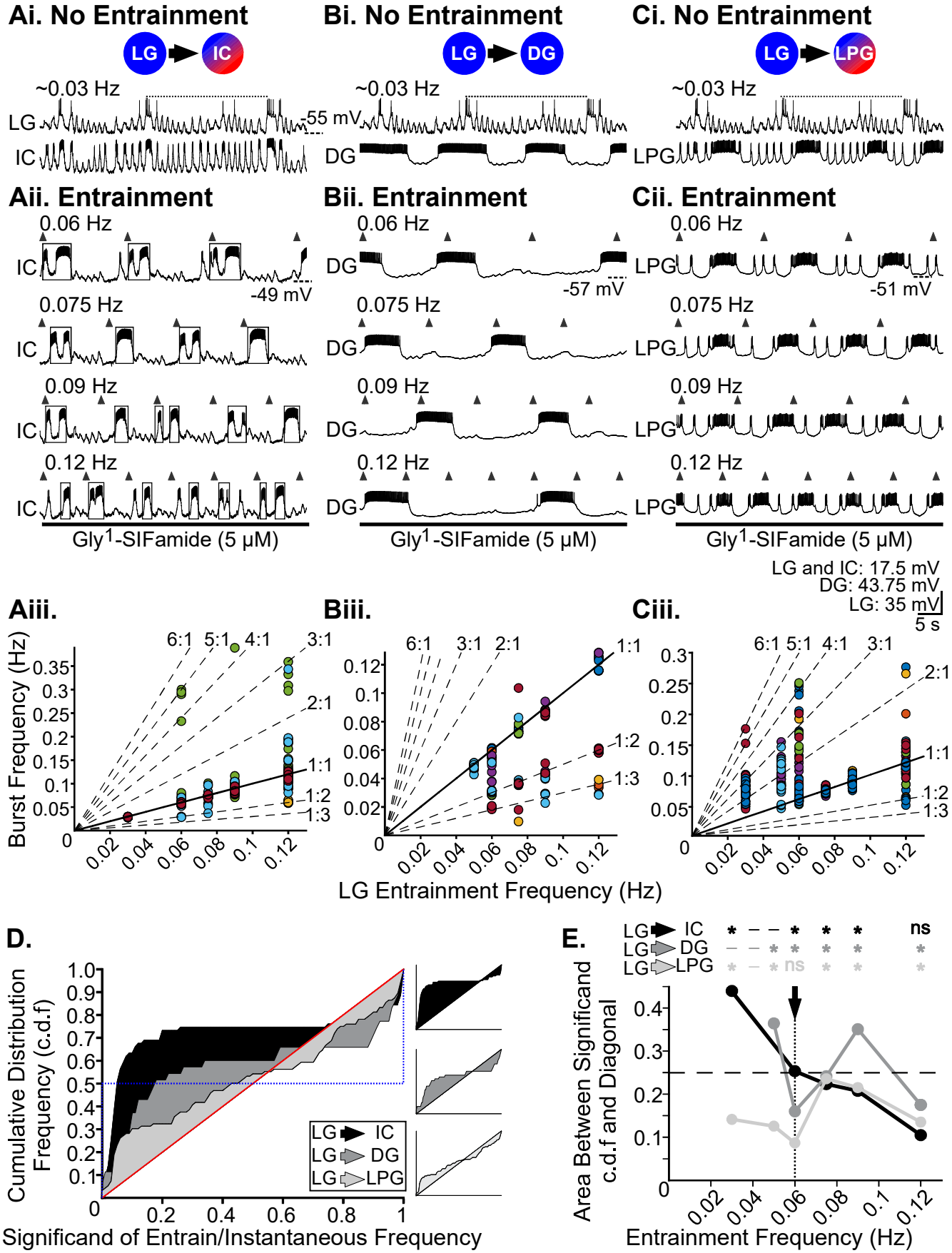

Figure 6
Fahoum and Blitz

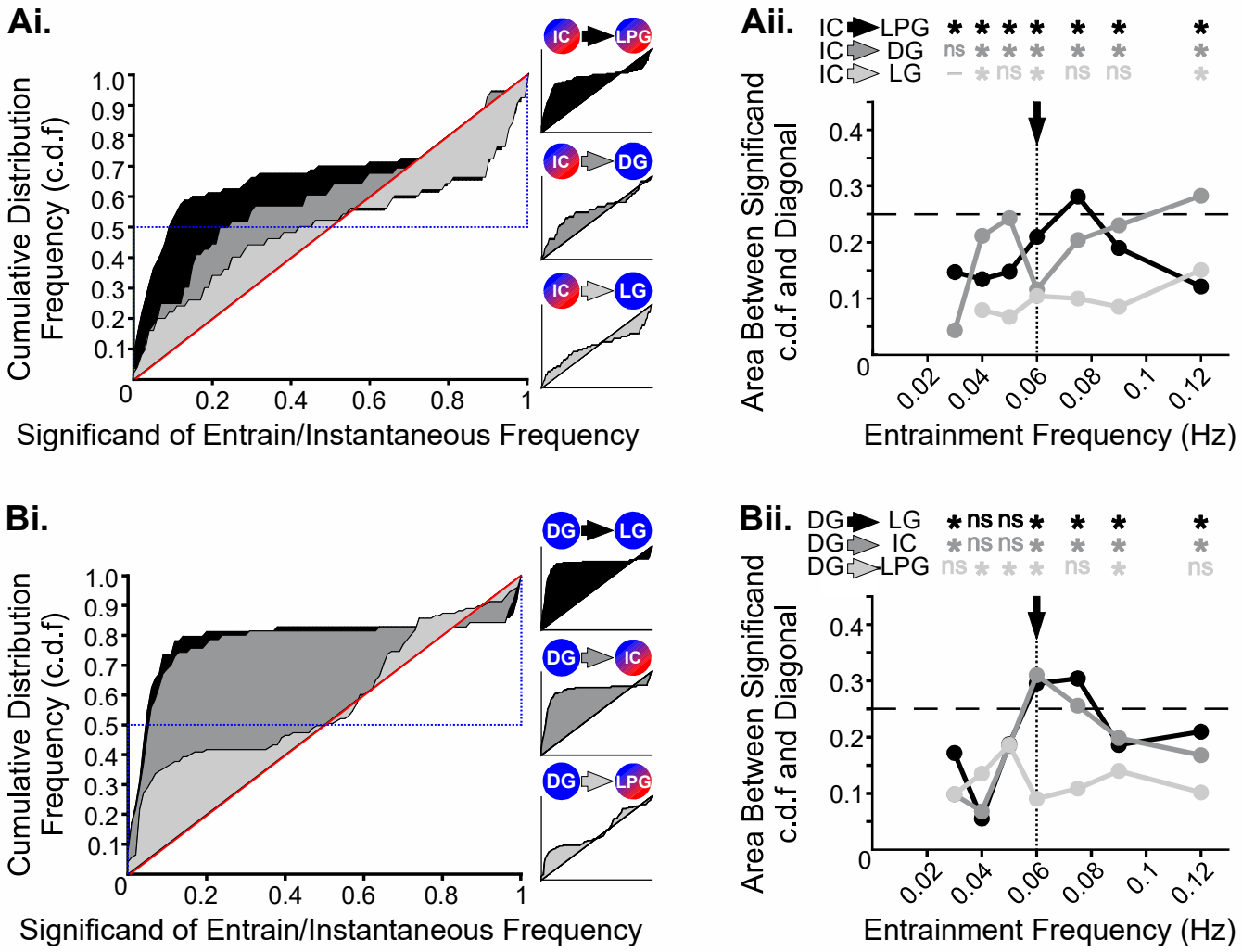

Figure 7
Fahoum and Blitz

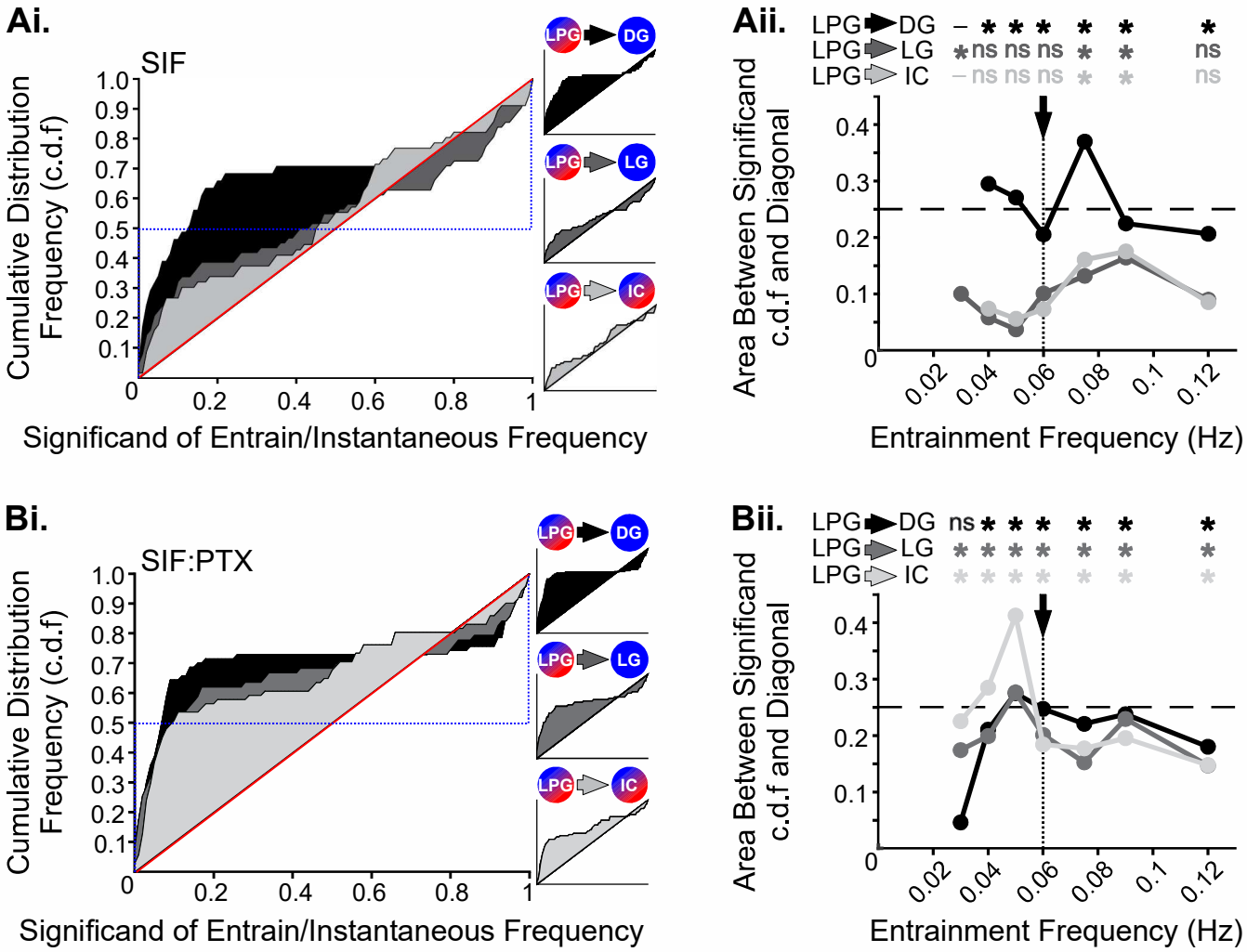

Figure 8
Fahoum and Blitz

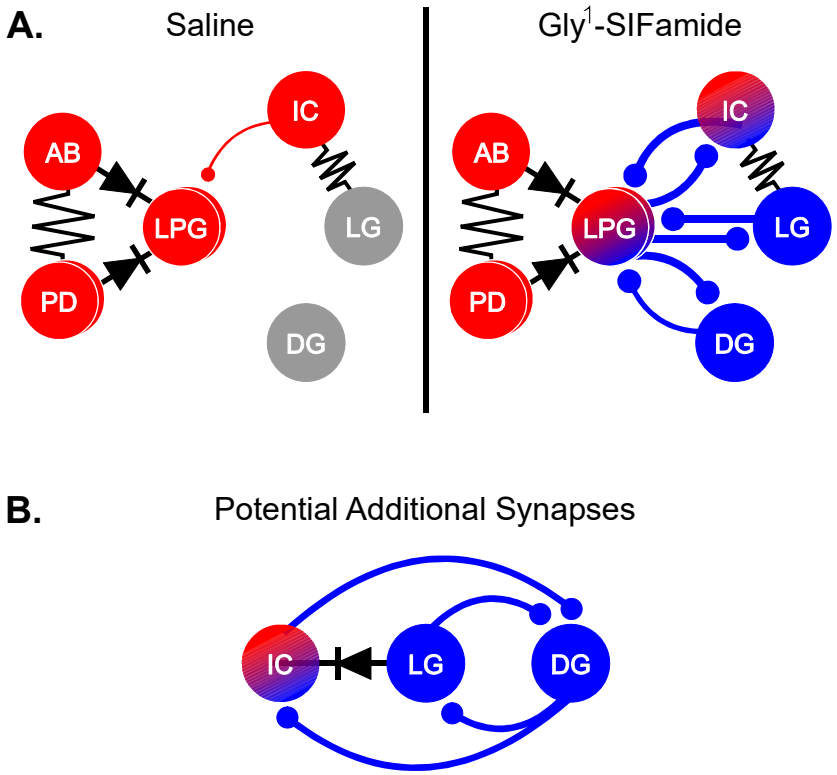

Figure 9
Fahoum and Blitz

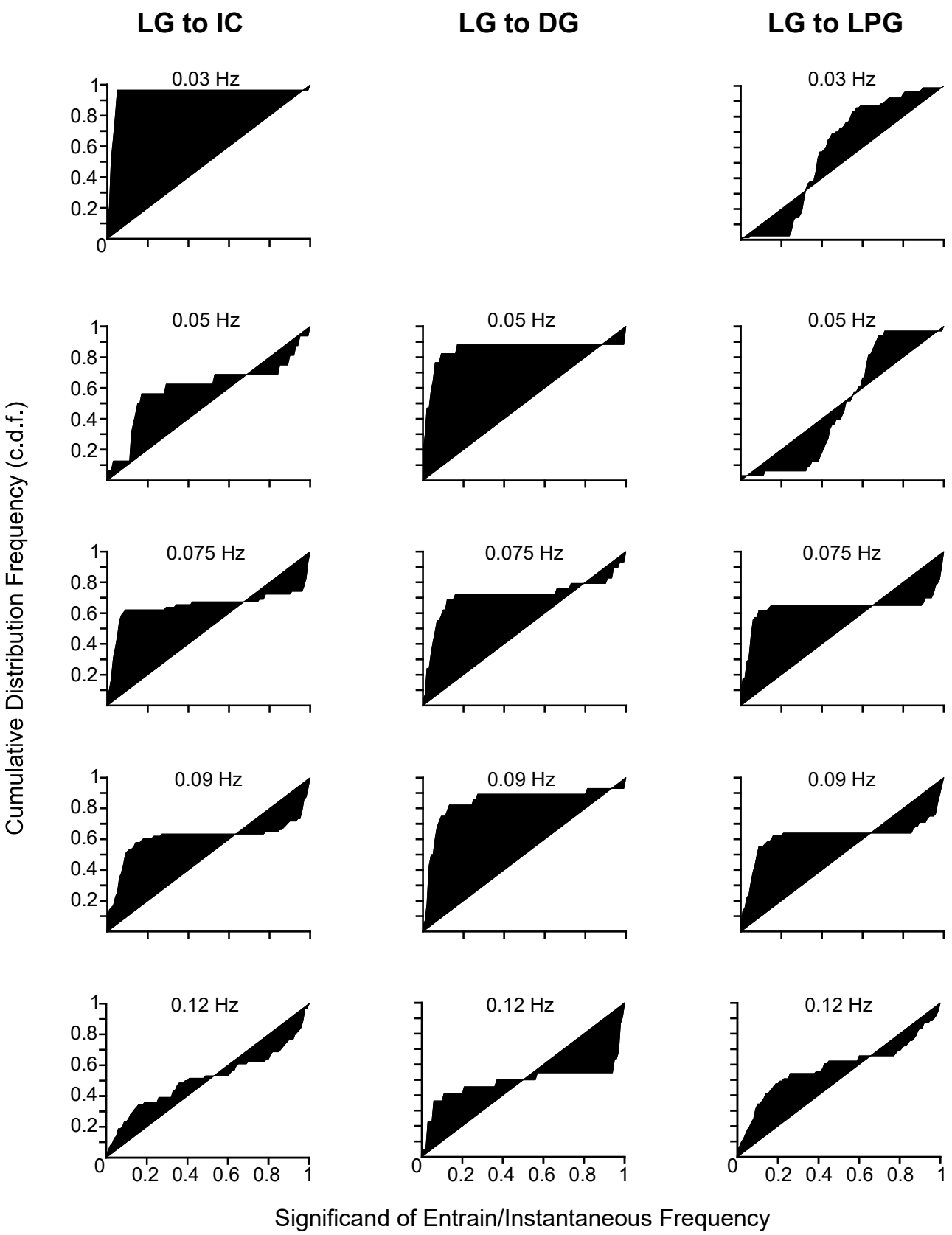

Supplemental Figure S1
Fahoum and Blitz

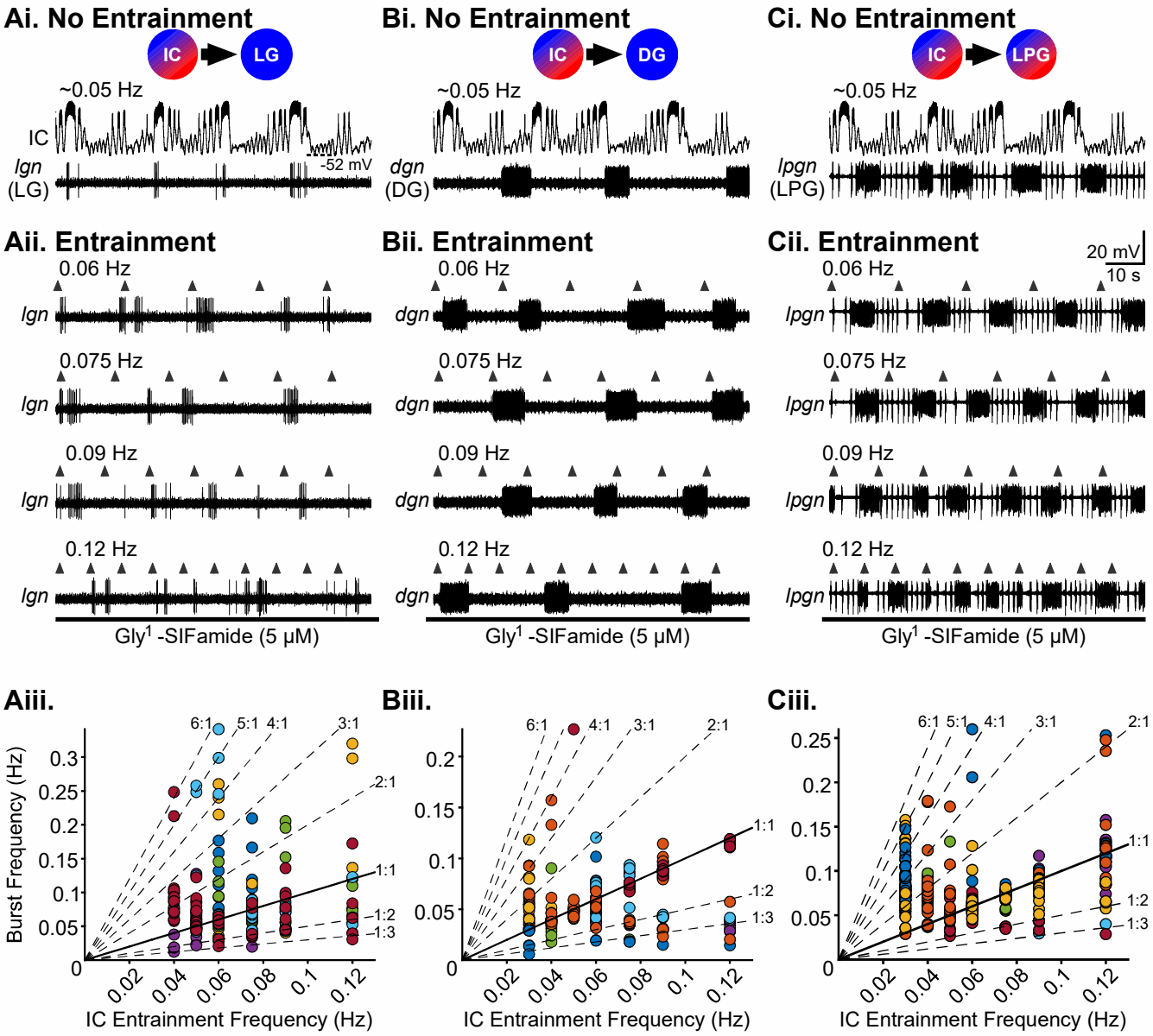

Supplemental Figure S2
Fahoum and Blitz

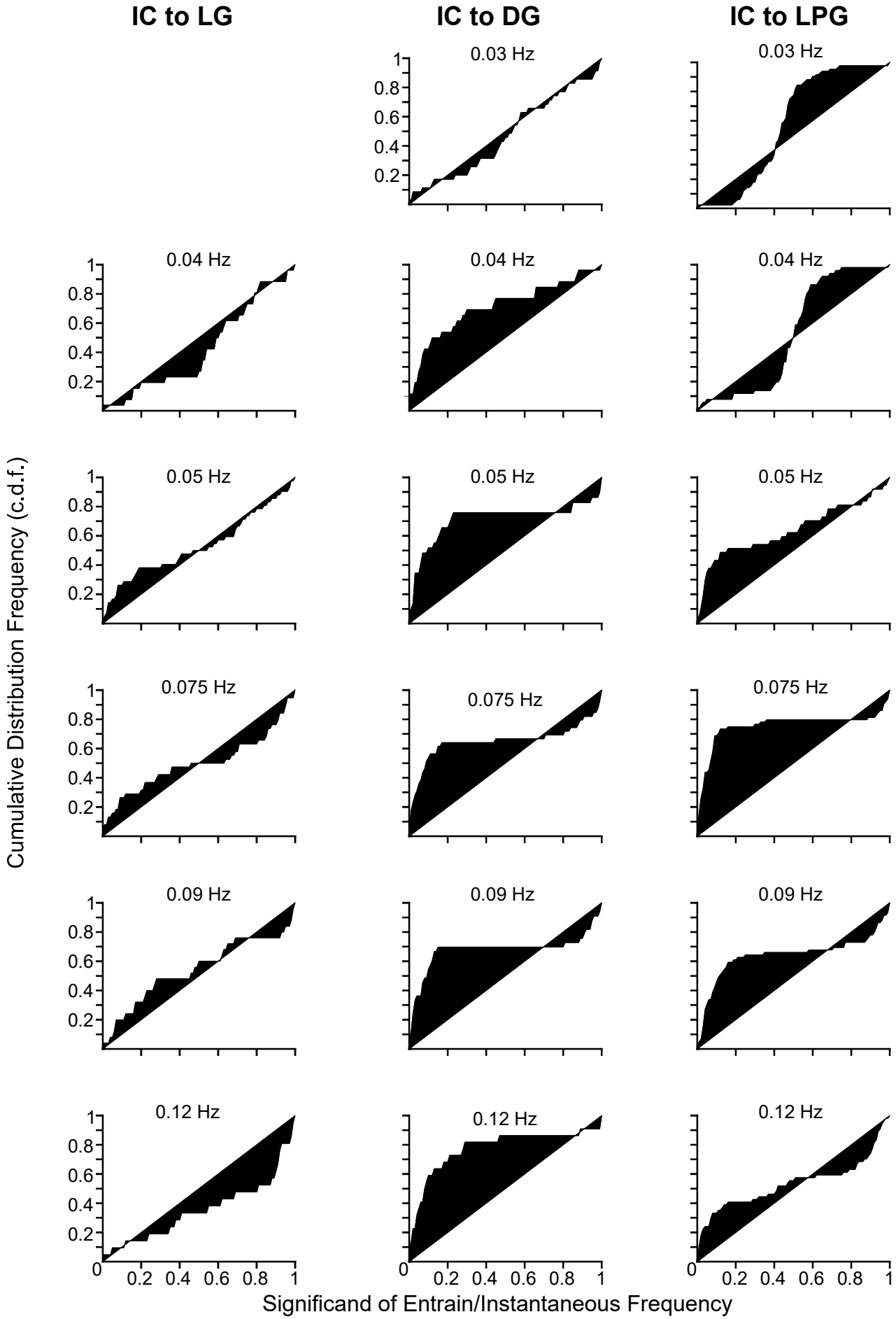

Supplemental Figure S3
Fahoum and Blitz

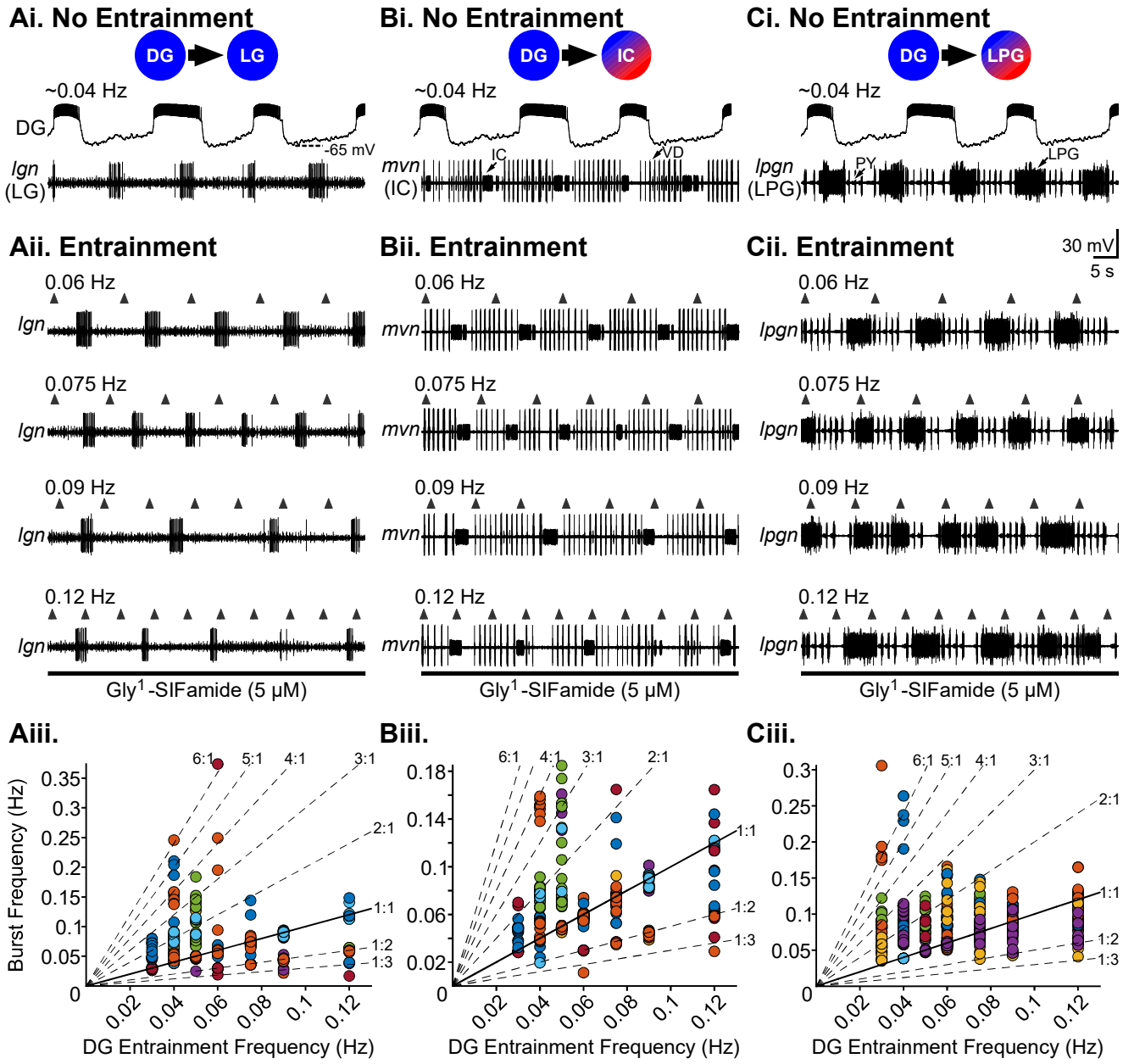

Supplemental Figure S4
Fahoum and Blitz

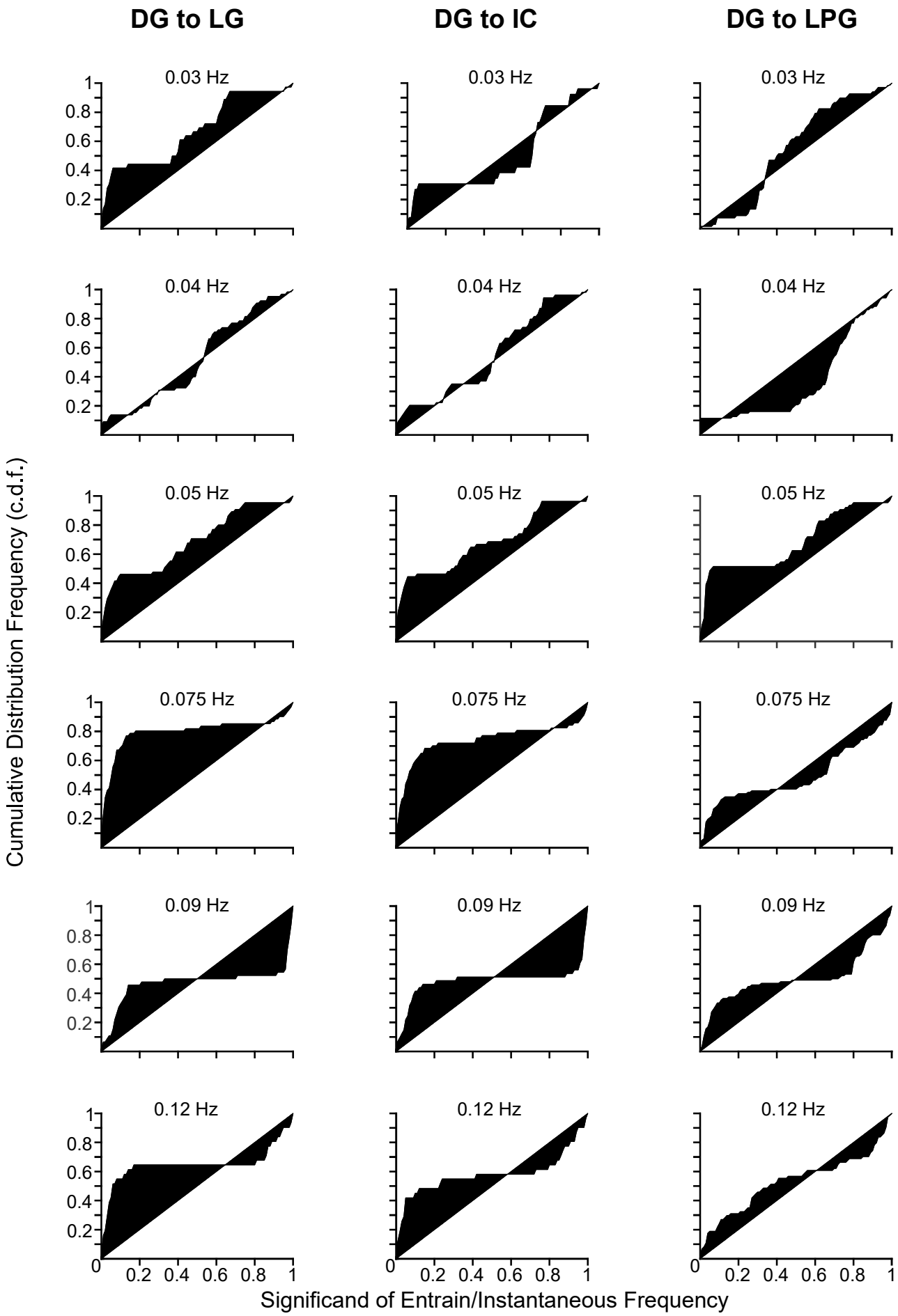

Supplemental Figure S5
Fahoum and Blitz

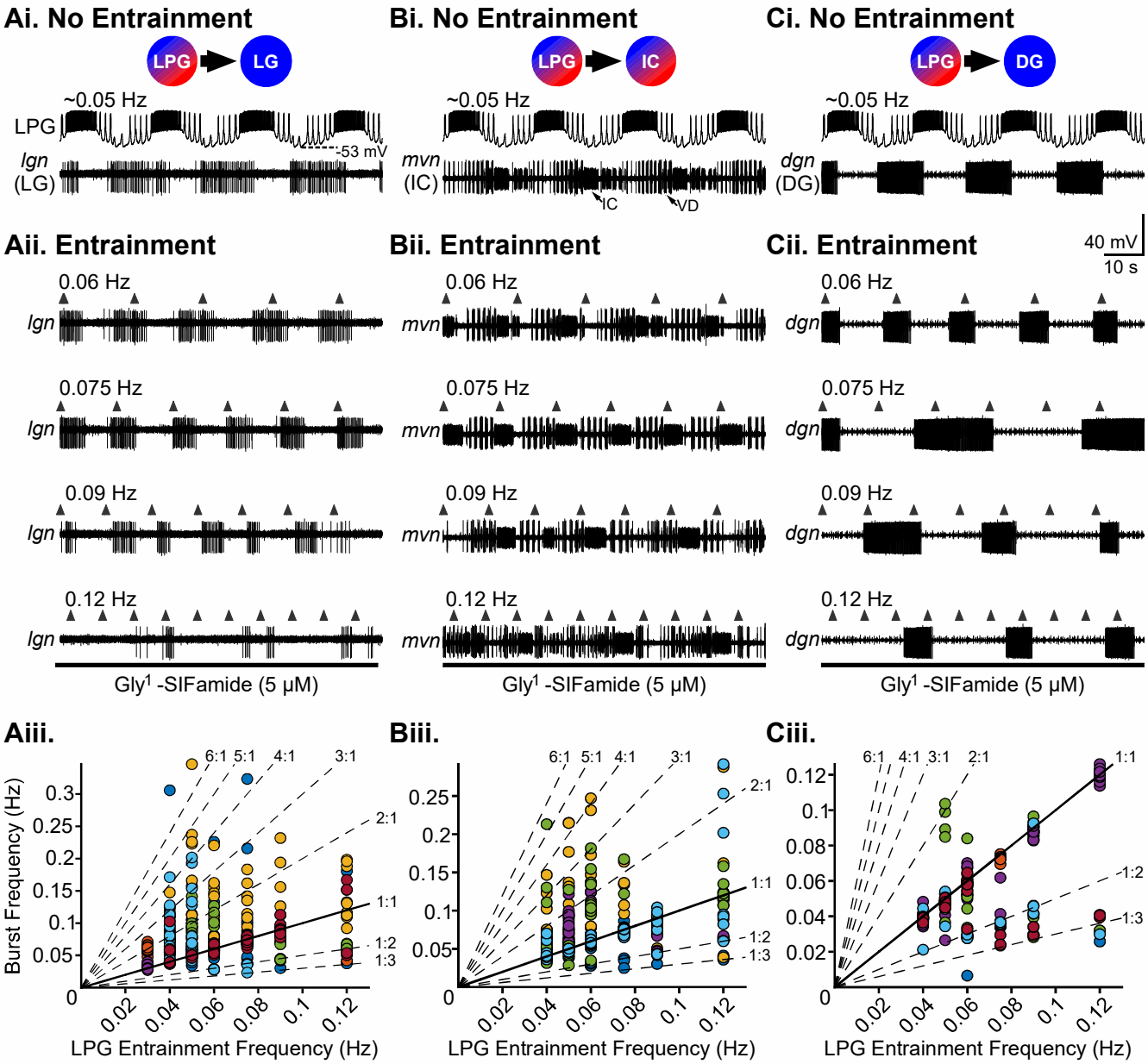

Supplemental Figure S6
Fahoum and Blitz

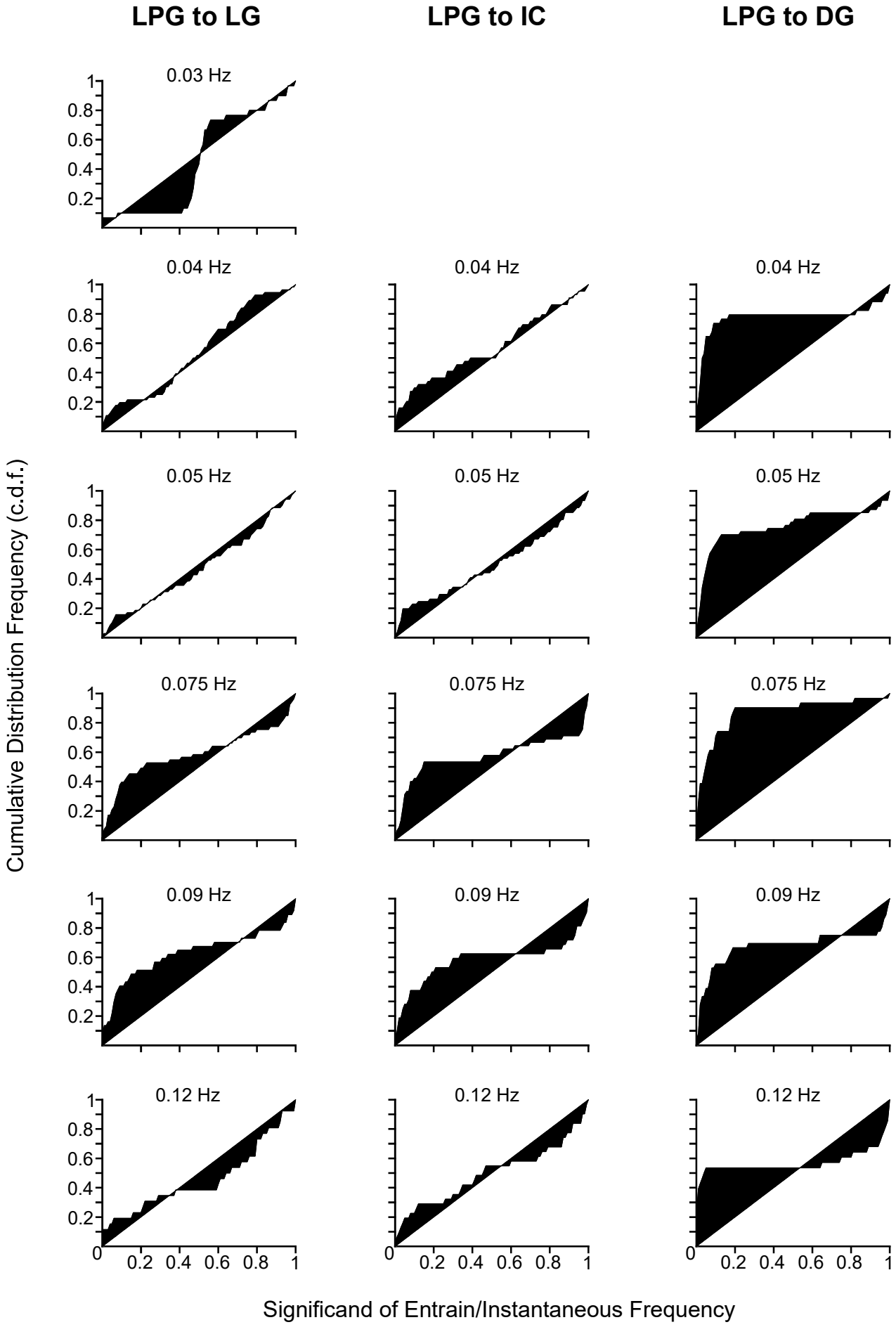

Supplemental Figure S7
Fahoum and Blitz

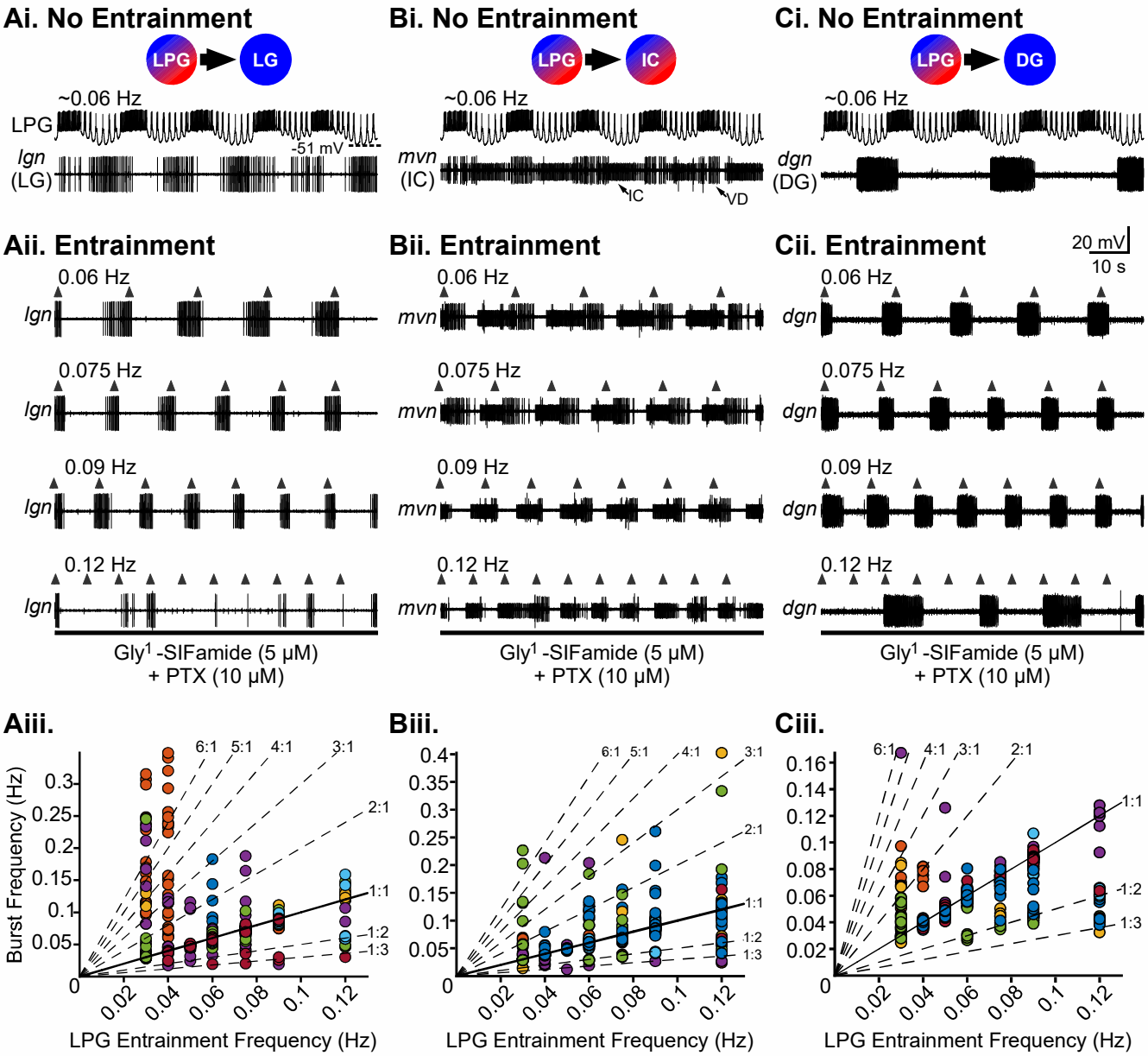

Supplemental Figure S8
Fahoum and Blitz

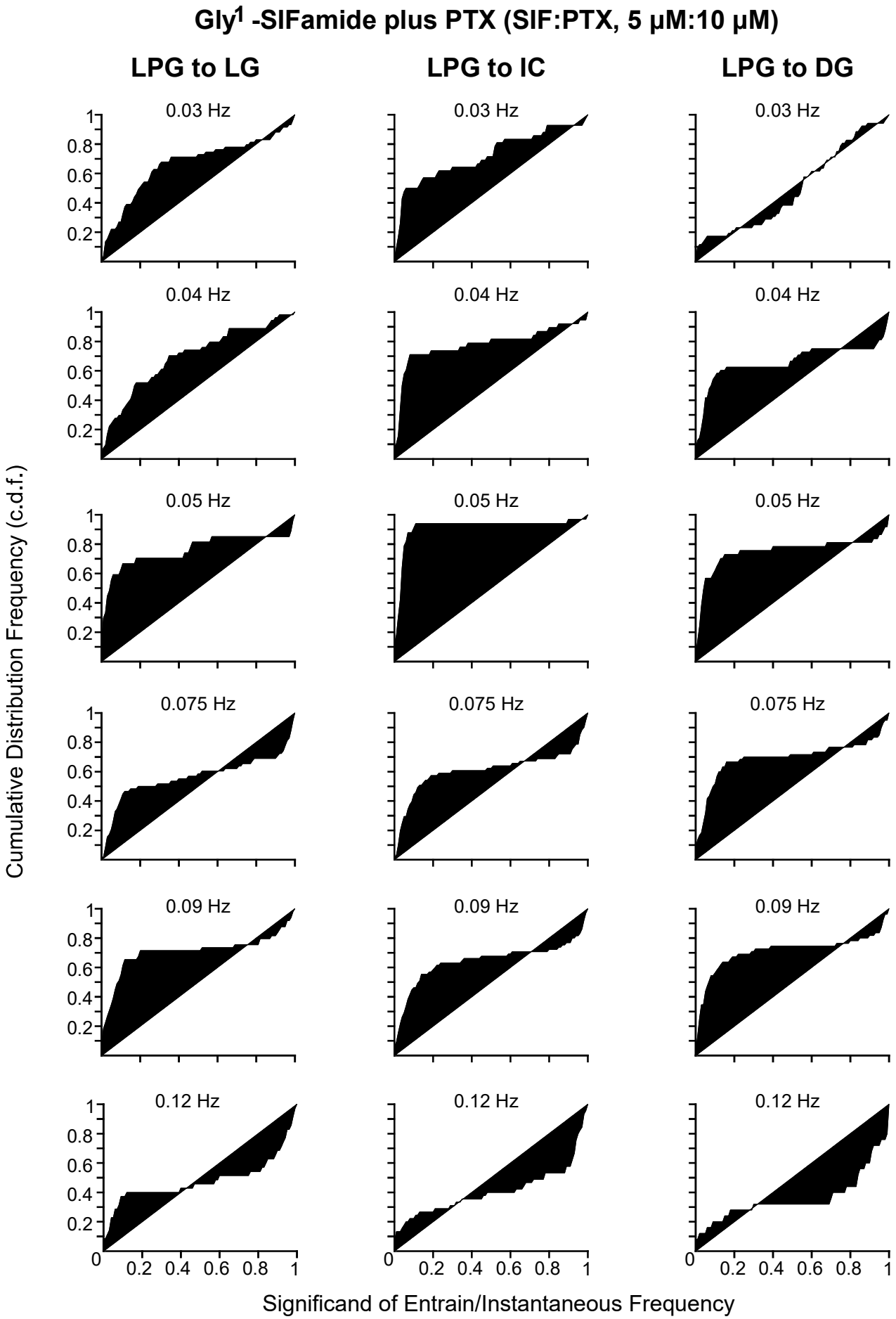

Supplemental Figure S9
Fahoum and Blitz